THE INSTITUTE OF SPACE AND ASTRONAUTICAL SCIENCE
YOSHINODAI, SAGAMIHARA, KANAGAWA 229-8510

ISAS RESEARCH NOTE

ISAS RN 694

Contributions to the IAU Colloquium 177 and the Conference on "X-ray Astronomy 1999"

F. Nagase, Y. Ueda, B. Paul, H. Negoro, M. Sugizaki,
H. Matsumoto, T.G. Tsuru, M. Takahashi, et al.

February 2000

I. IAU Colloquium 177: Pulsar Astronomy - 2000 and Beyond

Bonn, Germany, August 30 - September 3, 1999

II. X-Ray Astronomy 1999 - Stellar Endpoints, AGN, and Diffuse Background

Bologna, Italy, September 6 - 10, 1999

Contents

I. IAU Colloquium 177: Pulsar Astronomy - 2000 and Beyond

Bonn, Germany, August 30 - September 3, 1999

II. X-Ray Astronomy 1999 - Stellar Endpoints, AGN, and Diffuse Background

Bologna, Italy, September 6 - 10, 1999

5. "Short-Term Spectral Variations During X-Ray Flares in Black Hole Candidates and AGNS",
   H. Negoro

6. "The Population of Faint X-Ray Sources in the Galaxy and Their Contribution to the Galactic Ridge X-Ray Emission",
   M. Sugizaki, K. Matsuzaki, H. Kaneda, S. Yamauchi, K. Mitsuda and ASCA Galactic Plane Survey Team

7. "X-Ray Evidence of an AGN in M82",
   H. Matsumoto and T.G. Tsuru

8. "Variability of an Iron Line Profile and a Power-Law Continuum",
   K. Misaki, H. Kunieda, and Y. Terashima

9. "A New Event Analysis Method for the X-Ray Photo Count CCD",
   T.G. Tsuru, H. Awaki, K. Koyama, K. Hamaguchi, H. Murakami, M. Nishiuchi, M. Sakano and H. Tsunemi

Pulsar Astronomy — 2000 and Beyond
ASP Conference Series, Vol. 3 × 10^8, 1999
M. Kramer, N. Wex, and R. Wielebinski, eds.

ASCA Observations of the Crab-Like Pulsar PSR B0540−69

F. Nagase, T. Endo

The Institute of Space and Astronautical Science, 3-1-1 Yoshinodai, Sagamihara, Kanagawa 229-8510, Japan

M. Hirayama

Santa Cruz Institute for Particle Physics, University of California, Santa Cruz, CA 95064, U.S.A.

N. Kawai

The Institute of Physical and Chemical Research, 2-1 Hirosawa, Wako, Saitama 351-0198, Japan

M. Itoh

Faculty of Human Development, Kobe University, Tsurukabuto, Nada, Kobe 657-8501, Japan

Abstract. We report on the spectral and temporal properties of the 50 ms pulsar PSR B0540−69 using ASCA archival data obtained during 1993 to 1995. From the spectral analysis it was found that the spectra of the whole (nebular and pulsed) emission and pulsed emission in the range 1-10 keV can be represented by a single power law of photon index, $\Gamma = 2.00 \pm 0.02$ and $\Gamma_{\rm pulsed} = 1.7 \pm 0.3$ respectively. The parameters for pulse frequency change during 1993-1995 were obtained using the 9 pulse frequency measurements with ASCA. The parameters derived from the ASCA observations are consistent with the previous measurements, suggesting high stability of this pulsar, $\Delta\Omega/\Omega \lesssim 0.5 \times 10^{-7}$ over the past 10 years. These results confirm similarity of this pulsar with the Crab pulsar.

1. Introduction

The 50 ms pulsar PSR B0540−69 in the Large Magellanic Cloud was first discovered in soft X-ray band near the center of a synchrotron nebula (Seward et al. 1984). Follow-up ground-based observations revealed optical pulsations of magnitude $m_V \sim 22.5$ (Middleditch & Pennypacker 1985). This pulsar is faint (~ 0.4 mJy) in radio band, although the radio pulsation was detected from long time integration (Manchester et al. 1993). HST observations (Hill et al. 1997) confirmed the astrometric position of the pulsar given by Caraveo et al. (1992) and provided a high quality optical spectrum of the pulsar.

Table 1. Journal of ASCA observations of PSR B0540−69 and measurements of pulse frequencies.

ID	Observation Date	Exposure time (ks)	Epoch (MJD)	Pulse Frequency ν (Hz)	Error (μHz)
A	93/06/13	15.7	49151.589853	19.8356915	3.6
B	93/09/22	23.8	49252.080619	19.8340554	4.5
B&C*	—	—	49253.321078	19.8340355	0.7
C	93/09/24	36.8	49254.461630	19.8340170	2.0
D	94/10/01	7.2	49626.100997	19.8279677	8.9
D&E*	—	—	49627.132475	19.8279515	0.6
E	94/10/03	8.4	49628.130331	19.8279374	7.2
F	94/10/11	2.4	49636.378558	19.8277991	19.8
F&G*	—	—	49637.048671	19.8277903	1.4
G	94/10/12	8.5	49637.716262	19.8277812	11.2
H	94/11/07	3.8	49663.206701	19.8273635	15.1
I	95/11/07	36.6	50028.453569	19.8214242	0.9

* Pulse frequencies are determined by combining two adacent data sets with a few days separations for B&C, D&E, F&G.

A measurement of the braking index of $n = 2.02 \pm 0.01$ was reported by Nagase et al. (1990) from the X-ray pulse timing using the Ginga data. Deeter, Nagase & Boynton (1999; DNB ephemeris) recently derived more precise braking index of $n = 2.080 \pm 0.003$ for about 4 years from 1987 to 1991. In this paper, we report the results of spectral and timing analyses using ASCA archival data obtained in the period of 1993 to 1995.

2. Observations

During the perfomance verification phase of ASCA in 1993, a systematic survey of bright LMC regions including the pulsar PSR B0540−69 was performed. Several snap-shot observations of the source were performed in 1994 October to November to monitor the pulse frequency. During the observation of SN1987A in 1995 November, the pulsar was observed at the corner of the GIS field. Data for PSR B0540−69 were extracted from these archival observations are summarized in Table 1. The dataset C in the table was used for the spectral analysis, whereas all data listed in Table 1 were used for pulse timing analysis. Details of data reduction and analysis procedure are given elsewhere by Hirayama et al. (1999).

3. Energy Spectrum

A point-like X-ray source is detected clearly at the position of PSR B0540−69 in all the data sets. To derive the spectral parameters accurately we used data obtained on September 23-24, 1993 for spectral analysis, when the pulsar was observed at the nominal position in the GIS field and the exposure time is largest. The X-ray spectrum of the whole source is well represented by a single

Table 2. Pulse frequency parameters of PSR B0540-69 obtained from the present analysis are compared with those by Deeter et. al. (1999).*

Parameter	DNB ephemeris	This work
t_0 (MJD)	47700.0	49590.021711
ν_0 (Hz)	19.8593584982(52)	19.82855532(92)
$\dot{\nu}_0$ (10^{-10} Hz s^{-1})	$-1.8894081(10)$	$-1.88323(25)$
$\ddot{\nu}_0$ (10^{-21} Hz s^{-2})	3.7388(49)	3.77 ± 2.25
braking index n ..	2.0799(27)	2.11 ± 1.26

* Derived by fitting to the quadratic ephemeris, $\nu(t) = \nu_0 + \dot{\nu}_0 (t - t_0) + \frac{1}{2}\ddot{\nu}_0 (t - t_0)^2$. Values in the parenthesis are the errors in the last decades of each parameter.

power-law model of photon index, $\Gamma = 2.00 \pm 0.02$, with a small photoelectric absorption, corresponding to $N_{\rm H} = (4.3 \pm 0.2) \times 10^{21}$ cm^{-2}. This results in an X-ray luminosity of $L_{\rm X} = (1.16 \pm 0.03) \times 10^{37}$ erg s^{-1} in the energy range 1-10 keV, assuming the source distance to be 55 kpc.

The X-ray pulsations were clearly detected and the folded light curves show one broad pulse with a small dip on the top which is consistent with previous observations (e.g., Seward et al. 1984, Deeter et al. 1999). We made pulse-phase resolved spectroscopy and found that the photon index varies with pulse phase ranging from 2.0 to 2.2, while the photoelectric absorption remain constant. It is found from the phase resolved analysis that the pulsed emission can be represented by an absorbed single power-law model with photon index, $\Gamma_{\rm pulsed} = 1.7 \pm 0.3$ with an X-ray luminosity of $L_{\rm X,pulsed} = (2.9 \pm 0.3) \times 10^{36}$ erg s^{-1} in the 1-10 keV range. These are smoothly connected with the soft X-ray spectra derived from ROSAT in 0.1-2.4 keV range (Finley et al. 1993) and confirm the similarity of the nebular/pulsed spectra of this system with those of Crab nebular/pulsar system.

4. Pulse Timing Analysis

Local pulse frequencies derived from the 9 data sets are given in Table 1 together with the epoch of determination, where we adopted the mid-time of each observation as an epoch. We also derived pulse frequencies by combining two consecutive data sets of 1-2 days separation (B plus C, D plus E and F plus G) to get more accurate values of the pulse frequencies, as shown in the table. The resulting pulse frequencies are fitted by a quadratic function and the derived parameters are listed in Table 2. Residuals from the best-fit quadratic fit are plotted in the left panel of Figure 1.

The pulse frequency ephemeris derived with ASCA is consistent with that given by Deeter et al. (1999; DNB ephemeris), although the accuracy of determination is worse by about two orders of magnitude. This is because the data sampling of ASCA is sparse and the length of data interval is short. In addition the current analysis is limitted to the fit to locally determined pulse frequencies, while the DNB ephemeris was derived finally by pulse phase coherent analysis. Differences of the ASCA measurements of pulse frequencies to the DNB ephemeris are plotted in the right panel of Figure 1 together with those of the

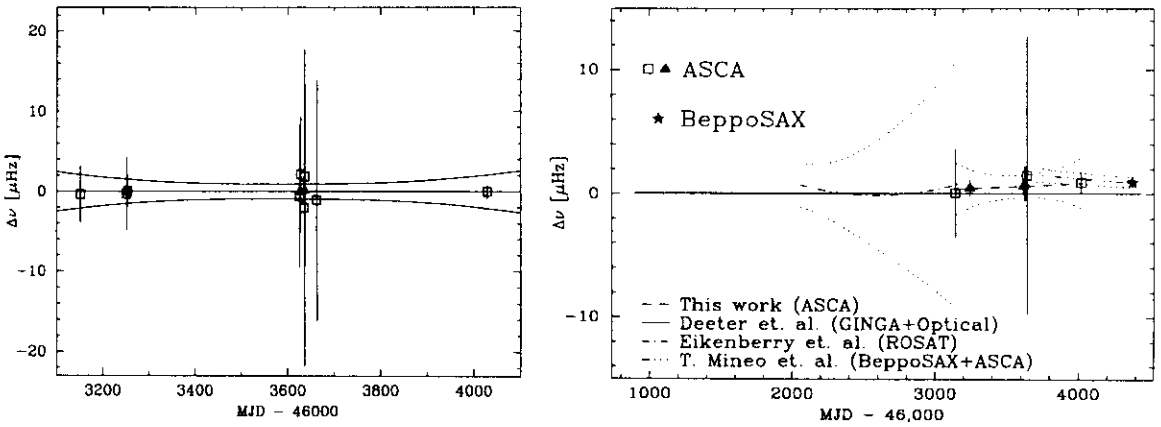

Figure 1. Left: Residuals from a quadratic ephemeris for pulse frequencies determined from ASCA observations of PSR B0540−69. Right: Differences of pulse frequencies and ephemeris of ASCA to the DNB ephemeris are plotted together with those of the ROSAT ephemeris (Eikenberry et al. 1998) and BeppoSAX pulse frequency (Mineo et al. 1999). The solid (left panel) and dashed/dotted (right panel) curves are the ±90 % significance regions of ephemeris solutions.

ROSAT ephemeris (Eikenberry et al. 1998) and the BeppoSAX pulse frequency (Mineo et al. 1999). This demonstrates that the stability of the neutron star spin in PSR B0540−69 is $\Delta\nu \lesssim 1$ μHz (or $\Delta\Omega/\Omega \lesssim 0.5 \times 10^{-7}$) over the past 10 years. This suggests that the braking index measured by DNB holds for about 10 years to the ASCA period and during this period PSR B0540−69 did not experience a large glitch as is seen in Vela pulsar. These confirm the Crab-pulsar like nature of this pulsar.

References

Caraveo, P. A., Bugnami, G. F., Mereghetti, S., et al. 1992, ApJ, 395, L103
Deeter, J. E., Nagase, F., & Boynton, P. E. 1999, ApJ, 512, 300
Eikenberry, S. S., Fazio, G. G., & Ransom, S. M. 1998, ApJ, 492, 754
Finley, J. P., Ögelman, H., Hasinger, G., & Trümper, J. 1993, ApJ, 410, 323
Hill, R. J., Dolan, J. F., Bless, R. C., et al. 1997, ApJL, 486, L99
Hirayama, M., Endo, T., Nagase, F., et al. 1999, in preparation
Manchester, R. N., Mar, D. P., Lyne, A. G., et al. 1993, ApJL, 403, L29
Middleditch J., & Pennypacker C. R. 1985, Nature, 313, 659
Mineo, T., Cusumano, G., Massaro, E., et al. 1999, AAp, 348, 519
Nagase, F., Deeter, J., Lewis, W., et al. 1990, ApJL, 351, L13
Seward, F. D., Harnden, F. R. Jr., & Helfand, D. J. 1984, ApJL, 287, L19

Pulsar Astronomy — 2000 and Beyond
ASP Conference Series, Vol. 3×10^8*, 1999*
M. Kramer, N. Wex, and R. Wielebinski, eds.

New *ASCA* Observations of two Anomalous X-ray Pulsars

B. Paul[1] , M. Kawasaki, T. Dotani, and F. Nagase

Institute of Space and Astronautical Science
3-1-1 Yoshinodai, Sagamihara, Kanagawa 229-8510, Japan

Abstract. New *ASCA* observations of two anomalous X-ray pulsars (AXP) 4U 0142+61 and 1E 1048.1-5937, made in 1998, when compared to earlier observations in 1994 show remarkable stability in the intensity, spectral shape and pulse profile. The energy spectra consist of two components, a power-law and a blackbody emission from the neutron star surface. In 1E 1048.1-5937, we have identified three epochs with different spin-down rates and discuss its implications for the magnetar hypothesis of the AXPs. We also note that the spin-down rate and its variations in 1E 1048.1-5937 are much larger than what normally can be produced by an accretion disc with very low mass accretion rate corresponding to its low X-ray luminosity.

1. Introduction

A set of X-ray pulsars are known to have remarkable similarity in their properties which are different from other binary or isolated X-ray pulsars (Mereghetti & Stella 1995). The properties common to most of these objects are a) pulse period in a small range of 5–12 s, b) monotonous spin down with $\dot{P}$ in the range of, $5 \times 10^{11} - 1.3 \times 10^{13}$ s, c) identical X-ray spectrum consisting of steep power-law ($\Gamma = 3 - 4$) and black body component (kT $\sim$ 0.5 keV), d) stable X-ray luminosity ($10^{34} - 10^{36}$ ergs s^{-1}) for years, e) faint or unidentified optical counterpart, and f) no evidence of orbital motion. The sources also have a galactic distribution, most of these are within $|b| \leq 0.5^\circ$ and all are probably young ($\sim 10^4$ yr) because of their association with SNR or molecular clouds. The objects in which all the properties mentioned above have been observed are 4U 0142+61, 1E 2259+586, 1E 1048.1-5937, 1RXS J170849.0-400910 and 1E 1841-045 (Kes 73).

Considering the strong similarity between these handful of sources, it has been proposed that they have same physical nature and different scenarios have been proposed to explain the observed properties. The prominent models are accretion from low mass binary companion (Mereghetti & Stella 1995), single neutron star accreting from molecular cloud or remnant of common envelope evolution (van Paradijs, Taam & van den Heuvel 1995; Ghosh, Angelini & White

[1]On leave from the Tata Institute of Fundamental Research, Homi Bhabha Road, Colaba, Mumbai 400005, India

1997) and extremely high magnetic filed neutron star radiating due to magnetic field decay (Thompson & Duncan 1996). Unlike the radio pulsars and rotationally powered X-ray pulsars, in the AXPs, the spin-down rate is not large enough to power the observed X-ray emission. The AXPs are in many respect also similar to the X-ray counterparts of the Soft Gamma-ray Repeaters (SGR).

Stability of the X-ray emission properties (spin-down rate, luminosity, spectral shape and pulse shape and fraction) is usually mentioned as one important aspect of the AXPs though one has to compare between observations made with different instruments for which the energy band, energy resolution and sensitivity are not identical. To make a rigorous comparison in the stability of the X-ray emission properties we have studied two AXPs with the *ASCA* with four years time difference between the observations. The aim was to critically examine the stability of the X-ray emission pattern and more pulse period measurements which may provide support to either the accretion powered or the magnetar hypothesis for these objects.

2. Observations and results

Both the sources were observed twice with *ASCA*, in 1994 & 1998 with about 4 years time difference between the two observations. The 1998 observations resulted in new measurement of pulse periods 8.688267 ± 0.000024 (4U 0142+61, epoch MJD = 51046.7) and 6.450815 ± 0.000002 (1E 1048.1+5937, epoch MJD = 51021.1). The pulse fraction, defined as ratio of the pulsed to total flux was calculated from background subtracted pulse profiles in the 0.5–10.0 keV band. Pulse fractions ($\sim$ 9% and $\sim$ 75% in 4U 0142+61 and 1E 1048.1-5937 respectively) and pulse shapes were found to be identical in both the observations. Light curves of the two sources did not show any intensity variations at minutes to days time scale. The pulse period measurements of 4U 0142+61 is rather scarce except for the last two years (Figure 1) and is consistent with a constant spin-down rate. The flux history of 4U 0142+61 shows only about 15% variability around the average value, and multiple measurements with the same instrument of *ASCA* and *Beppo-SAX* (Israel et al. 1999) gave almost identical flux. In the source 1E 1048.1-5937, including the 1998 *ASCA* observation (Figure 1), three different epochs with different spin-down rates of $1.5 \pm 0,5 \times 10^{-11}$, 1.67×10^{-11}, and 3.29×10^{-11} s s^{-1} are clearly identified. In 1E 1048.1-5937, the over all intensity during the two *ASCA* observations and one *Beppo-SAX* observation in between are within 10% of the average value. The flux measurements from the previous observations are about a factor 3 higher than the recent measurements. But for non-imaging instruments, contribution from the nearby bright source η-Carina may have resulted in overestimation of the flux.

For both the sources, a spectral model consisting a power-law and a blackbody component with line of sight absorption results in acceptable fit. For 4U 0142+61, the power-law photon index is 3.8 and temperature of the black body component is 0.39 keV. Same for 1E 1048.1-5937 are 3.0 and 0.56 keV respectively. For details of the spectral fitting and values of all the spectral parameters for the two observations, see Paul et al. (1999). In the *ASCA* observations of both the sources separated by 4 years we have found that the overall intensity and spectral parameters have remarkable stability.

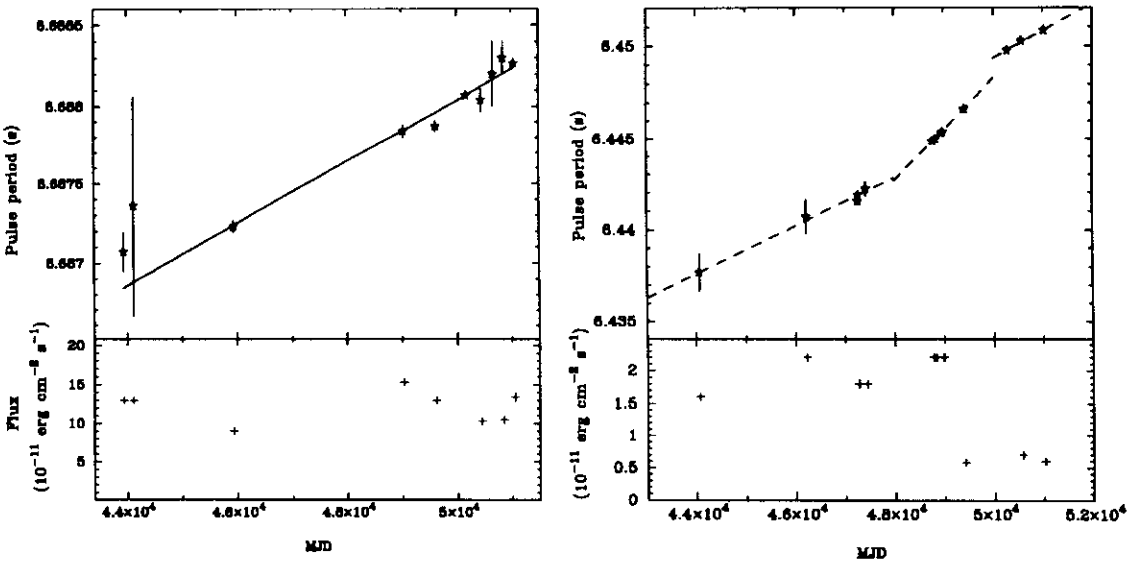

Figure 1. Pulse period and flux history of 4U 0142+61 and 1E 1048.1-5937. The pulse period measurements with *ASCA* are marked with filled symbols.

3. Accretion torque in the common envelope evolution model

In the common-envelope evolution model of the AXPs, the pulsar is rotating near its equilibrium period. The spin-down is explained with the assumption that the mass accretion rate from the disc decreases slowly on viscous time scale with corresponding increase in the equilibrium period. For 1E 1048.1-5937, which has a pulse period of 6.5 s and luminosity of 6.3×10^{33} erg s^{-1} for a distance of 3 kpc (or in a more favourable case, 7×10^{34} erg s^{-1}, if the source is at a distance of 10 kpc), even if we assume that all of the X-ray emission is a result of disc accretion, the accretion torque is only 1.1×10^{31} (or 1.2×10^{32}) gm cm^2 s^{-2}. To achieve the observed spin-down rate, the negative torque required to be imparted onto the neutron star is $I\dot{\Omega} = 4.9 \times 10^{33}$ gm cm^2 s^{-2}. This is a factor of 450 (or 40) larger than the accretion torque, and in the common envelope evolution model, a negative dimensionless torque of this magnitude is required to spin-down the pulsar at the observed rate. In other words, the spin-down rate of this source is much larger than what can be achieved with disc accretion onto a neutron star with a luminosity of less than 10^{35} erg s^{-1}.

4. Magnetar model

1E 1048.1-5937 shows clear deviation from a constant spin-down. Two scenarios have been proposed which can explain the changing spin-down rate even when the overall braking is due to the ultra-strong magnetic filed. Melatos (1999) showed that for reasonable neutron star parameters, a radiative precession effect may take place which can give the observed spin-down variations with time scale of about 10 years. Heyl and Hernquist (1999) have proposed that the spin-down variations can be explained as glitches (similar to radio pulsars) superposed on constant spin-down. A clustering of the pulse period of 10 sources (7 AXPs and

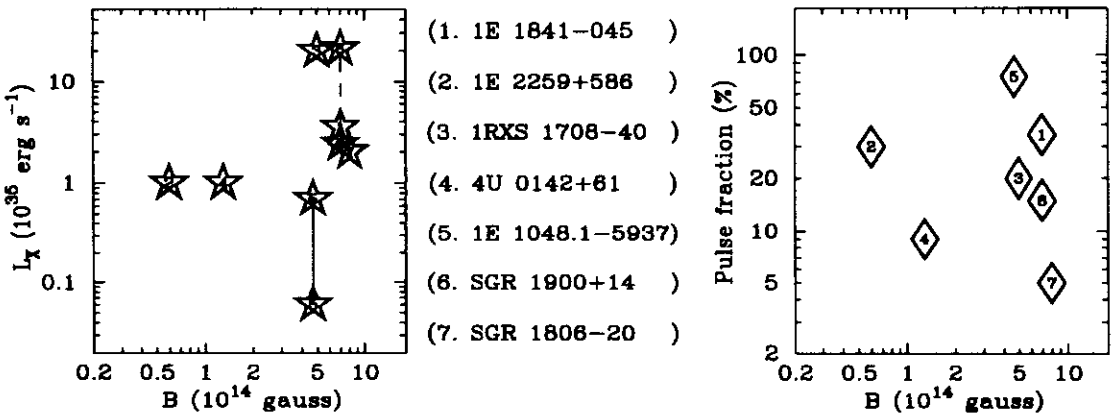

Figure 2. The X-ray luminosity and pulse fraction of the AXPs and SGRs are plotted against the magnetic field strength assuming that these objects are magnetars. Intensity variations and uncertainty in distance are shown by multiple points for some objects.

3 SGRs) in the 5-12 s range also needs to be addressed, when the magnetars are expected to be alive in X-ray until they have slowed down to a pulse period of about 70 s (Duncan & Thompson 1992).

If the pulsation is due to confinement of the heat in the magnetic polar regions by the magnetic field, a correlation between magnetic field strength and pulse fraction is possible. This will be somewhat smeared by the the orientation of the spin and magnetic axes with respect to the line of sight of individual sources. In the magnetar model, there are two mechanisms by which X-rays can be generated. If the X-ray emission is powered by decaying magnetic filed, $L_x \propto B^4$ (Thompson & Duncan 1996). Alternately, if X-ray generation is due to particle acceleration by Alfven waves resulting from small scale fracture of the crust, $L_x \propto B^2$. The X-ray luminosity and pulse fraction of five confirmed AXPs and two SGR sources are shown in Figure 2. against the magnetic filed strength. Though there is uncertainty in the luminosity of some sources, a 2nd or 4th power correlation between L_X and B does not seem to be present. There is also no correlation between pulse fraction and the magnetic field.

References

Duncan, R. C., & Thompson, C. 1992, ApJ, 392, L9
Ghosh, P., Angelini, L., & White, N. E. 1997, ApJ, 478, 713
Heyl, J. S., & Hernquist, L. 1999, MNRAS, 304, L37
Melatos, A. 1999, ApJ, 519, L77
Mereghetti, S., & Stella, S. 1995, ApJ, 442, L17
Israel, G. L., et al., 1999, A&A, 346, 929
Paul, B., Kawasaki, M., Dotani, T., & Nagase, F. 1999, ApJ(in preparation)
Thompson, C. & Duncan, R. C. 1996, ApJ, 473, 322
van Paradijs, J., Taam, R. E., & van den Heuvel, E. P. J. 1995, A&A, 299, L41

Pulsar Astronomy — 2000 and Beyond
ASP Conference Series, Vol. 3 × 10⁸, 1999
M. Kramer, N. Wex, and R. Wielebinski, eds.

Detection of Pulsed X-ray Emission from The Fastest Millisecond Pulsar PSR B1937+21 with ASCA

Motoki Takahashi[1], Shinpei Shibata[1], Ken'ichi Torii[2], Yoshitaka Saito[3], Nobuyuki Kawai[2,4], Masaharu Hirayama[5], Tadayasu Dotani[3], Shuichi Gunji[1] and Hirohisa Sakurai[1]

[1] *Department of Physics Yamagata University, Kojirakawa, Yamagata 990-8560, Japan*

[2] *NASDA TKSC SURP, 2-1-1 Sengen, Tsukuba, Ibaraki 305-8505, Japan*

[3] *The Institute of Space and Astronautical Science, Sagamihara, Kanagawa 229, Japan*

[4] *The Institute of Physical and Chemical Research (RIKEN), Wako, Saitama 351-01, Japan*

[5] *Santa Cruz Institute for Particle Physics University of California, Santa Cruz, CA 95064*

Abstract. We report the first detection of the pulsed X-ray emission from the fastest millisecond pulsar known PSR B1937+21 (P =1.558msec) with ASCA. The pulsar is detected as a point source above $\sim$ 1.7keV, with no nebulosity indicated. The source flux in the energy band 2–10keV is found to be $f = 4.3 \times 10^{-13}$erg s^{-1} cm^{-2}, which corresponds to the luminosity of $L_{\rm x} = 4\pi D^2 f \approx 6.6 \times 10^{32} (D/3.6{\rm kpc})^2$ erg s^{-1}, where D is the distance, and correspond to $\approx 6 \times 10^{-4}$ of the rotation power of the pulsar. The pulsation is found at the period predicted by the radio ephemerides with very narrow primary peaks, the width of which is about 1/16 phase $\approx 100\mu$s near the time resolution limit (61μs) of the observation. The pulsed luminosity within the primary peak (1/16 phase interval) is found to be $f_p = 4.0 \times 10^{-12}$erg s^{-1} cm^{-2}. Although there may be a secondary peak, its statistical significance is too low to identify. Spectra of the whole source region and the primary peak are fitted by power law models to give photon indices of about unity for both.

1. Introduction

The fastest *millisecond pulsar* PSR B1937+21 can own the strongest magnetic field at the light cylinder (l-c), which can exceeds the value of the Crab pulsar, $\sim 10^6$G, while their surface fields $\sim 10^8$G are four orders of magnitude smaller than the typical values for the ordinary pulsars $\sim 10^{12}$G. There are two proposed emission regions in the pulsar magnetosphere, the polar gap near the surface and the outer gap near the l-c. The field strength of the fastest millisecond pulsars is similar to the Crab value for the outer gap, and it is much smaller for the polar

gap. Therefore, detection of the magnetospheric emission from the millisecond pulsars is certainly expected to contribute to the debate about the location of particle acceleration in the pulsar magnetosphere.

2. Observation and Results

The fastest millisecond pulsar known is PSR B1937+21 (Backer et al. 1982) and was observed with the ROSAT, given only an upper bound flux (Verbunt et al. 1996). We observed PSR B1937+21 with ASCA (Tanaka et al. 1994) on 15–17 November 1997 with the duration of 97,140 s. And we detected the X-ray emission in the energy bands higher than $\sim$ 1.7keV; we give the results of the spatial, temporary and spectral analysis (Takahashi et al. 1998).

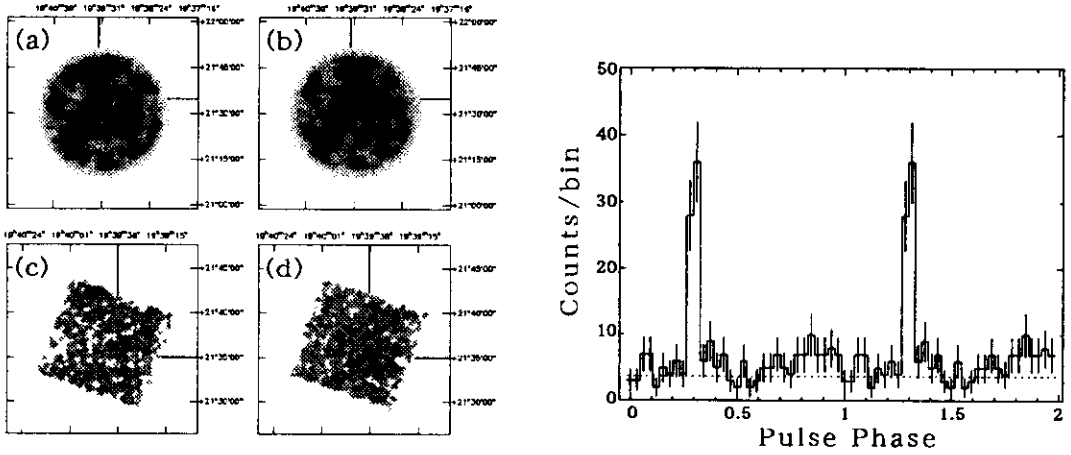

Figure 1. Left: X-ray images of PSR B1937+21 obtained with ASCA. (a) GIS Soft Band (0.7–2 keV), (b) GIS Hard Band (2–10 keV), (c) SIS Soft Band (0.5–2 keV), (d) SIS Hard Band (2–10 keV). The radio position is indicated by the vertical and horizontal lines in the images. Right: Integrated pulse profile of PSR B1937+21 in the GIS 1.7 - 6.5 keV band. The dashed line indicates the background level, 3.67 counts/bin, where the 32 phase bins are used.

Acknowledgments. This work is supported in part by a Grant-in-Aid for Scientific Research (10117203) from the Ministry of Education, Science, and Culture in Japan.

References

Backer, D.C., Kulkarni, S.R., Heiles, C., Davis, M.M., & Goss, W.M., 1982, Nature, **300**, 615

Takahashi, M., Shibata, S., Torii, K., Saito, Y. & Kawai, N., 1998, IAUC, **7030**, 3

Tanaka, Y., Inoue, H. & Holt, S. S. 1994, PASJ, **46**, L37

Verbunt, F., Kuiper, L., Belloni, T., Johnston, H. M., De Bruyn, A. G., Hermsen, W., & Van Der Klis, M., 1996, A&A, **311**, L9

TRANSIENT BE STAR BINARY SYSTEMS

F. Nagase [1]

1) The Institute of Space and Astronautical Science, 3-1-1 Yoshinodai, Sagamihara, Kanagawa 229-8510, Japan

ABSTRACT In this paper we review current status of X-ray observations of transient Be star binary systems. An overview of remarkable discoveries of transient X-ray pulsars in the last few years is given and general properties common to transient Be star binary pulsars are summarized. A few interesting topics revealed from recent observations are also presented.

KEYWORDS: eclipsing binaries; interstellar dust; X-ray pulsars; X-ray sources.

1. INTRODUCTION

X-ray binaries containing neutron stars or black holes are classified into two types, the High Mass X-ray Binaries (HMXB) or Low Mass X-ray Binaries (LMXB) depending on the mass of the companion star. Most of the HMXBs show pulsations due to strong dipole magnetic field and mass accretion onto the magnetic poles at the neutron star surface. Bildsten et al. (1997) tabulated 44 X-ray pulsars in their review article. However, within a few years after their review, a dramatic rush of pulsar discoveries has been continuing, and the total number of accreting X-ray pulsars is about 80 at presnt (see e.g., Nagase 1999). Among them about a dozen wind-fed high mass X-ray binaries, four low mass X-ray binary pulsars and six anomarous X-ray pulsars are included. The rest three quadrants show a transient nature and more than half of them are identified to be massive Be star binaries. Thus the Be star X-ray binaries represent the largest sub-class of massive X-ray binaries. It seems a good assumption that all the transient X-ray pulsars are Be star binary systems, even though identification for some of them has not been done yet and occasionally it is difficult due to large extinction for the sources located in the Galactic plane near the center (see e.g., Coe 1999 for review of optical observations of Be star systems). Hereafter in this paper I designate this class of transient (Be star) X-ray binary pulsars as a TrXBP, regardless of the indentification of the Be star companion.

The pulse periods of TrXBPs (and every classes of X-ray pulsars) distribute uniformly in the range of a few seconds to a thousand seconds with a few exceptions as shown in Figure 1. This is in good contrast to the radio pulsars, the pulse periods of which are more narrowly distributed below a few seconds. It will be worthy to note that more than 20 TrXBP were discovered from Magellanic Clouds in the last

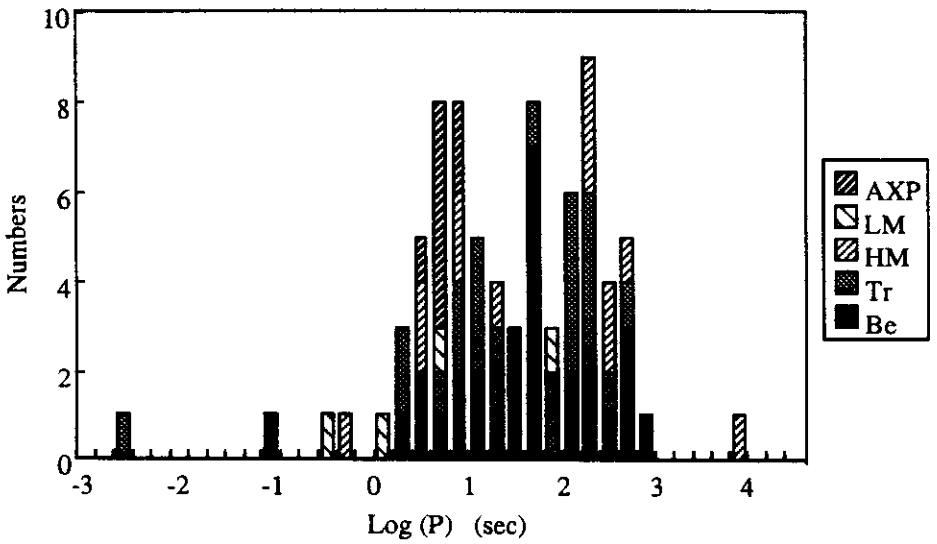

FIGURE 1. Distribution of pulse periods in accreting X-ray pulsars.

few years, in contrast to the fact that only three accreting pulsars were known for the past two decades. This rush of pulsar discoveries in LMC/SMC owes to the ideal line-up of X-ray observatories, ROSAT, ASCA, BeppoSAX, and XTE.

In the next section I summarize the general X-ray properties of TrXBPs. In section 3, I present some recent topics, such as (1) pulsar survey in Magellanic Clouds and investigation of X-ray source population in LMC/SMC, (2) Discoveries of TrXBPs lead by ROSAT Galactic plane survey, and (3) detection of soft-excess feature in the spectra of TrXBPs and consideration of the origin of the soft-excess feature.

2. X-RAY PROPERTIES OF TRANSIENT X-RAY BINARY PULSARS

Main X-ray properties common to TrXBPs, which are mostly Be star binaries, are

- Complex X-ray pulse profiles, depending on the energy bands and X-ray luminosity,
- Random pulse period change with the rate of change often correlating to the luminosity change,
- Simple, featureless power law spectrum with a weak iron fluorescent line, and
- Correlation between the binary orbital period and the pulsar spin period.

Some of the TrXBPs with a Be-star companion show regularly recurrent outbursts which take place at the periastron passage of the neutron satr. Occasionally some TrXBPs exhibit giant outbursts that ocur regardless of the orbital phase which

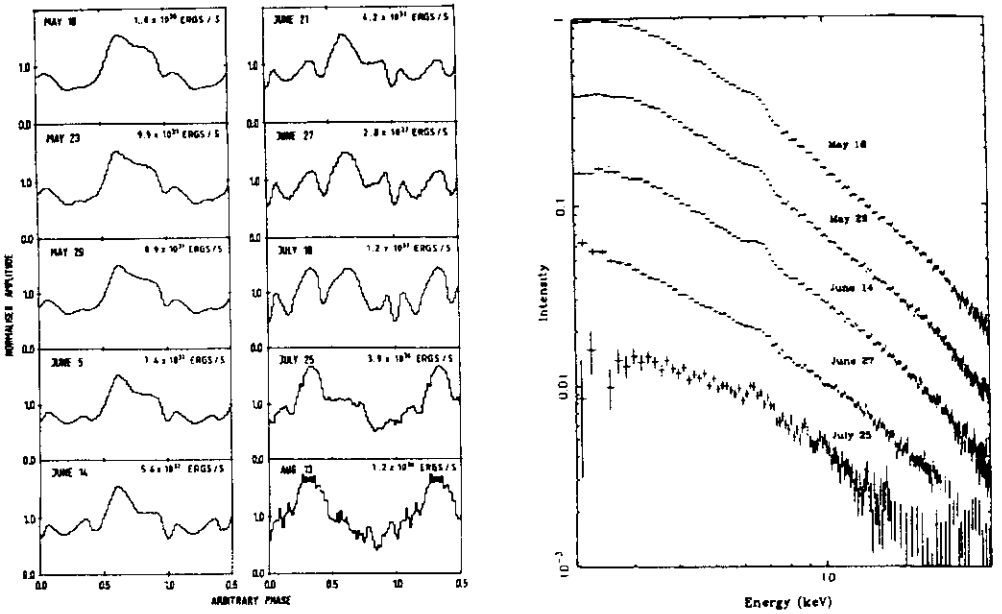

FIGURE 2. Changes of pulse profile and energy spectrum in a Be star X-ray binary pulsar EXO 2030+375 along with an outburst decay (taken from Parmar et al. 1989b and Renoulds et al. 1993).

may cause an extremely large expansion of the circumstellar disk. As mentioned in the previous section, pulse periods of TrXBPs distribute widely from ~ 3 s to 1000 s. The pulse profiles are fundamentally broad with a sinusoidal shape. However, they often exhibit complex change of features, including a multi-peak feature, a sharp dip at some pulse phase, according to the change of observed energy bands and X-ray luminosity during the observation. An example is shown in the left panel of Figure 2 where the complex change of pulse profile is clearly seen along the decay of an outburst in EXO 2030+375 (Parmar et al. 1989b). This figure shows almost every faces of pulse profiles so far observed in TrXBPs.

The trends of pulse period change in TrXBPs are complex and differ from source to source (see Bildsten et al. 1997). In general, there is a tendency that the neutron star spin rate is accelerated during outbursts, when the mass accretion rate increases and an accretion disk might be formed surrounding the neutron star. On the other hand the spin rate is decelerated during quiescent phases, when mass accretion from the Be star companion cease and the disk formed shrinks (see e.g., Nagase 1989). Occasionally a correlation between the rate of change in the pulse periods and the X-ray luminosity is observed in an outboursts along with the evolution of the outburst. During the declining phase of the 1985 outburst of EXO 2030+375, the correlation of $-\dot{P}_{spin} \propto L^{1.08-1.35}$ was measured (Parmar et al. 1989a), which

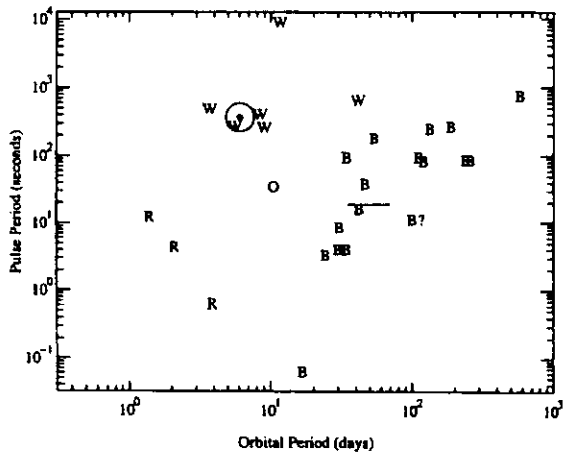

FIGURE 3. Pulse period versus orbital period of X-ray binary pulsars taken from Corbet et al. (1999).

was approximately consistent with the theory of accretion torque in disk-fed pulsars developed at the time (e.g., Ghosh and Lamb 1979).

Energy spectra of TrXBPs exhibit a hard power law of a photon index $\Gamma \sim 1$ with an exponential high energy cutoff at 15-30 keV. This feature in spectrum is common to accreting X-ray pulsars where mass accretion is halted by a strong magnetic field and the mass flow is channelled to the magnetic poles thus leading X-ray emission from accretion columns on the magnetic poles. There is a tendency that the spectral photon index changes with luminosity, usually hard at low luminosity. It has been known that wind-fed pulsars, such as Vela X-1, Cen X-3, and GX 301−2, exhibit a strong fluorescent line at 6.4 keV due to reprocessing by circumstellar matter, either stellar winds or an accretion disk. On the contrary, the flouorescent iron line in TrXBPs is relatively weak and often show broad line features (see e.g., White et al. 1983, Nagase 1989). An example of such spectral features is shown in the right panel of Figure 2 which was derived from the EXOSAT observation of an outburst in 1985 (Reynolds et al. 1993)

A correlation between the spin period and the orbital period of TrXBPs was discovered by Corbet (1986). The correlation diagram, so called "Corbet diagram" was useful at that time to discriminate the TrXBPs ("B" in Fig. 3) from Roche lobe overflow sources ("R" in Fig. 3) and wind accretion sources ("W" in Fig. 3) when both the spin and orbital periods are determined. With new orbital period measurements available mostly with RXTE/ASM monitoring, the boundary between TrXBPs and high mass wind-fed pulsars tend to become unclear (see Fig. 3 taken from Corbet et al. 1999). For a TrXBP, XTE J1855−026 (marked by a circled dot in Fig 3), Corbet et al. (1999) prefer the interpretation of a wind accretion pulsar rather than a Be star binary pulsar from the position on the Corbet diagram, although the nature of the companion star is not identified yet.

3. RECENT TOPICS

Several interesting findings on TrXBPs have been reported recently from observations with ROSAT, ASCA, BeppoSAX, and RXTE. The topics presented in this section are:

- Survey of Magellanic Clouds with ROSAT and discoveries of many TrXBPs with ASCA, BeppoSAX, and RXTE,
- Discoveries of TrXBPs lead by the systematic Galactic plane survey with ROSAT and ASCA and temporarily from RXTA/ASM all sky monitoring, and
- Detection of a soft-excess feature in the energy spectra of TrXBPs, especially from the sources in SMC.

3.1. Survey of Magellanic Clouds

Extensive surveys of the LMC and SMC regions were performed with ROSAT and more than 500 X-ray sources in LMC (Pietsch and Kahabka 1992) and 248 sources in SMC (Kahabka et al. 1999) were catalogued. Variabilities of 27 LMC X-ray sources were studied by Haberl and Pietsch (1999) using the ROSAT observations between 1990 and 1994. Details of the results of ROSAT LMC survey were presented by Haberl (1999) in this conference. Complete compilation and optical identification for the X-ray sources in LMC/SMC regions were performed in a series of papers by Schmidtke et al. (1994), Cowley et al (1997), and Schmidtke et al. (1999). Using spectral parameters estimated by two colors hardness ratios, Kahabka et al. classified 60 % of the detected 248 SMC sources into super-soft sources (SSS), X-ray binaries, supernova remnants (SNR), foreground stars,and background AGNs. About half of them were identifies to be X-ray binaries.

Recently more than 20 TrXBPs were discovered in the LMC/SMC regions (see e.g., Nagase 1999) from ROSAT, ASCA, BeppoSAX and RXTE observations. Yokogawa et al. (2000a) conducted a systematic analysis of the ASCA survey data of SMC region and found coherent pulsations from 12 sources among 39 sources detected with ASCA. Most of them were found to exhibit long-term flux variability, suggesting that they are TrXBPs. They also found that these TrXBPs can be clearly seperated from SNRs and other class of sources using the hardness ratio analysis (see Fig. 4).

It is remarkable that very few LMXBs were discovered so far from the SMC in contrast to the recent tremendous discoveries of TrXBPs. Thus the number ratio of HMXBs to LMXBs in SMC is strikingly different to our Galaxy where the population of LMXBs is larger than that of HMXBs as suggested by Schmidtke et al. (1999) and Yokogawa (1999). This implies that the SMC has been more active than our Galaxy in massive star formation. Since HMXBs are relatively young it is suspected that strong star formation activity in the SMC took place in the recent past, several million years ago.

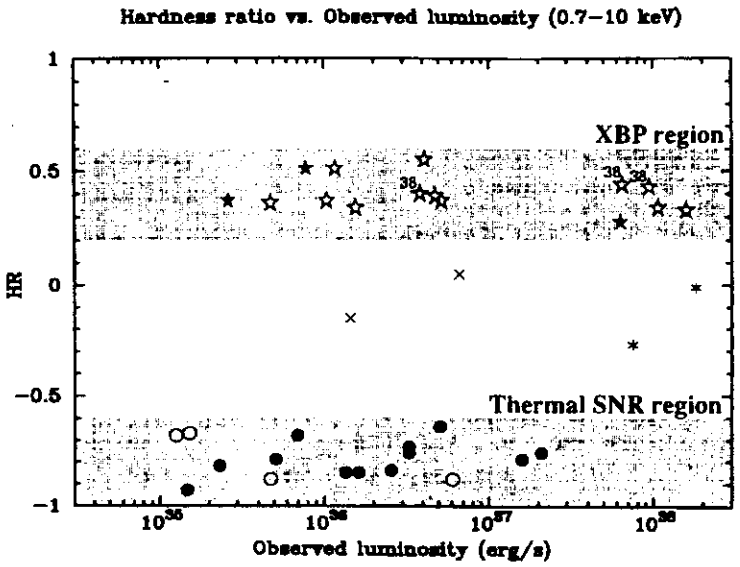

FIGURE 4. Hardness ratio versus luminosity of SMC/LMC sources taken from Yokogawa et al. (1999). Solid symbols represent LMC sources and open symbols represent SMC sources. The stars represent identified X-ray pulsars and the circles represent identified supernova remnants. Two asterisks in between XBP region and SNR region are black hole candidates and two crosses are Clab-like pulsars.

3.2. New Transients in Galactic Plane

In addition to the TrXBPs listed in the table of Bildsten et al. (1997), more than a dozen of TrXBPs were discovered from the Galactic plane observations with ASCA, BeppoSAX and RXTE. These sources are listed in Table 1 together with references.

It will be worthy to note that the discoveries of pulsations from three ROSAT sources among the TrXBPs in Table 1 were based on the ROSAT Galactic plane survey and optical identifications of these sources by Motch et al. (1997). The three ROSAT sources, RX J0812.4−3114, RX J0440.9+4431, and RX J1037.5−564 were readily identified to the Be binary systems, LS 992, BSD 24-491, and LS1698, respectively in the table compiled by Motch et al. (1997). From the RXTE observations of these sources, Reig and Roche (1999a, 1999b) discovered coherent pulsations. These sources show pulse profiles and energy spectra typical to TrXBPs as were described in section 2. An outburst recurrence period of about 80 d period was recently observed from RX J0812.4−3114/LS 992 system (Corbet & Peele 2000). Assuming that the recurrent outbursts are due to the periastron passage of the neutron star in the eccentric orbital around the Be star companion, this source is a typical TrXBP with the correlation between the spin perid and the orbital period on the Corbet diagram (Corbet 1986).

TABLE 1. X-ray pulsars recently discovered in the Galaxy and not cited in the table of Bildsten et al. (1997).

Source	l	b	Period(s)	Ref.[a]
SAX J1808.4−3658	355.395	−8.161	0.00249	1
SAX J0635+0533	206.151	−1.043	0.0338	2
XTE J1946+274	63.204	1.392	15.83	3
RX J0812.4−3114	249.578	1.543	31.8851	4
XTE J1906+09	42.561	1.047	89.17	5
AX J1820.5−1434	16.478	0.060	152.26	6
1SAX J1324.4−6200	306.793	0.609	170.84	7
RX J0440.9+4431	159.849	−1.2791	202.5	8
AX J1749.2−2725	1.707	0.106	220.38	9
XTE J1858+034	36.789	−0.068	221.0	10
SAX J2103.5+4545	87.130	−0.691	358.6	11
XTE J1855−026	31.102	−2.088	361.1	12
1SAX J1452.8−5949	317.645	−0.463	437.4	13
AX J170006−4157	344.0	0.2	714.5	14
RX J1037.5−5647	285.349	1.433	860	8

[a] References for pulsation discoveries: 1, Wijnands and van der Klis 1998, 2, Cusumano et al. 2000, 3, Smith et al. 1998, 4. Reig & Roche 1999a, 5, Marsden et al. 1998, 6, Kinugasa et al. 1998, 7, Angelini et al. 1998, 8, Reig & Roche 1999b, 9, Torii et al. 1998, 10, Remillard et al. 1998, 11, Hulleman et al. 1998, 12, Corbet et al. 1999, 13, Oosterbroek et al. 1999, 14, Torii et al. 1999.

3.3. Soft-Excess in Spectra of TrXBPs

A feature of excess intensities at energy below 1 keV in the spectrum over the extrapolation of a power low spectrum fitted to the higher energy has been reported from various sub-class of X-ray pulsars except for TrXBPs. The soft excess feature is considered to be a common propertiy in the spectra of anomalous X-ray pulsars (e.g., Mereghetti 1999) and the excess emission is usually fitted by a blackbody of temperature $kT = 0.4 - 0.7$ keV. Some LMXBs, such as Her X-1 and 4U 1626−67, show a soft excess feature in their spectra (e.g., McCray et al. 1982, Dal Fiume et al. 1998, Endo et al. 2000 for Her X-1 and Angelini et al. 1995, Orlandini et al. 1998 for 4U 1626−67). Evidence of such a soft excess feature has also been reported from HMXBs, LMC X-4 (Woo et al. 1996) and SMC X-1 (Wojdowski et al. 1998) from the combined analyses of ROSAT and Ginga data.

Such a clear soft excess feature, however, has not been reported so far from TrXBPs, because most of Galactic TrXBPs are subjected to heavy soft X-ray absorption and furthermore X-ray missions prior to ASCA did not have agood efficiency for a wide energy range from below 1 keV to 10 keV. Recently, clear exapm-

Cusumano G., Maccarone, M.C., Nicastro, L., Sacco, B., Kaaret, P. 2000, ApJ, in press
Dal Fiume, D., et al. 1998, A&A, 329, L41
Endo, T., Nagase, F., Mihara, T. 2000, PASJ, accepted
Ghosh, P., Lamb, F.K. 1979, ApJ, 234, 296
Haberl, F. 1999, in this Proceedings
Haberl, F., Pietsch, W. 1999, A&A, 344, 521
Hughes, J.P. 1994, ApJ, 427, L25
Hulleman F., in't Zand, J.J.M., Heise, J. 1998, A&A, 337, L25
Kahabka, P., Pietsch, W., Fillipovic, M.D., Haberl, F. 1999, A&AS, 136, 81
Kohno, M. Yokogawa, J., Koyama, K., 2000, PASJ, accepted
Kinugasa K., et al. 1998, ApJ, 495, 435
Marsden D., Gruber, D.E., Heindl, W.A., Pelling, M.R., Rothschild, R.E. 1998, ApJ, 502, L129
McCray, R.A., et al. 1982, ApJ, 262, 301
Mereghetti S., 1999, in *The neutron Star - Black Hole Connection*, NATO Advanced Study Institute, in press.
Motch C., Haberl, F., Dennel, K., Pakull, M., Janot-Pacheco, E. 1997, A&A 323, 853
Nagase, F. 1989, PASJ, 41, 1
Nagase, F. 1999, in the Proceedings of *Japanese-German Workshop on High Energy Astrophysics*, eds. W. Becker and M. Itoh, (MPE Report 270), p. 160
Oosterbroek, T., et al. 1999, A&A, 351,
Orlandini, M., et al. 1998, ApJ, 500, L163
Parmar, A.N., et al. 1989a, ApJ, 338, 359
Parmar, A.N., White, N.E., Stella, L. 1989b, ApJ 338, 373
Paul, B., et al. 1999, in this Proceeding
Pietsch, W., KahabkaP. 1992, in *Lecture Notes in Physics 416: New Aspects of Magellanic Cloud Research* eds. B. Baschek, G. Klare, K. Beuermann, p. 59
Reig, P., Roche, P. 1999a, MNRAS, 306, 95
Reig, P., Roche, P. 1999b, MNRAS, 306, 100
Remillard, R., et al. 1998, IAUC 6826
Reynolds, A.P. Parmar, A.N., White, N.E. 1993, ApJ, 414, 302
Schmidtke, P.C., et al. 1994, PASP, 106, 843
Schmidtke, P.C., et al. 1999, AJ, 117, 927
Smith D.A., et al. 1998, IAUC 7014
Torii K., et al. 1998, ApJ, 508, 854
Torii K., Sugizaki, M., Kohmura, T., Endo, T., Nagase, F. 1999, ApJ, 523, L65
White N.E., Swank J.H., Holt S.S. 1983, ApJ, 270, 711
Wijnands R., van der Klis, M. 1998, Nature, 394, 344
Wojdowski, P., Clark, G.W., Levine, A.M., Woo, J.W., Zhang, S.N. 1998, ApJ, 502, 253
Woo, J.W., Clark, G.W., Levine, A.M., Corbet, R.H.D., Nagase, F. 1996, ApJ, 467, 811
Yokogawa, J., et al. 2000a, ApJ, in press
Yokogawa, J., et al. 2000b, ApJ, accepted

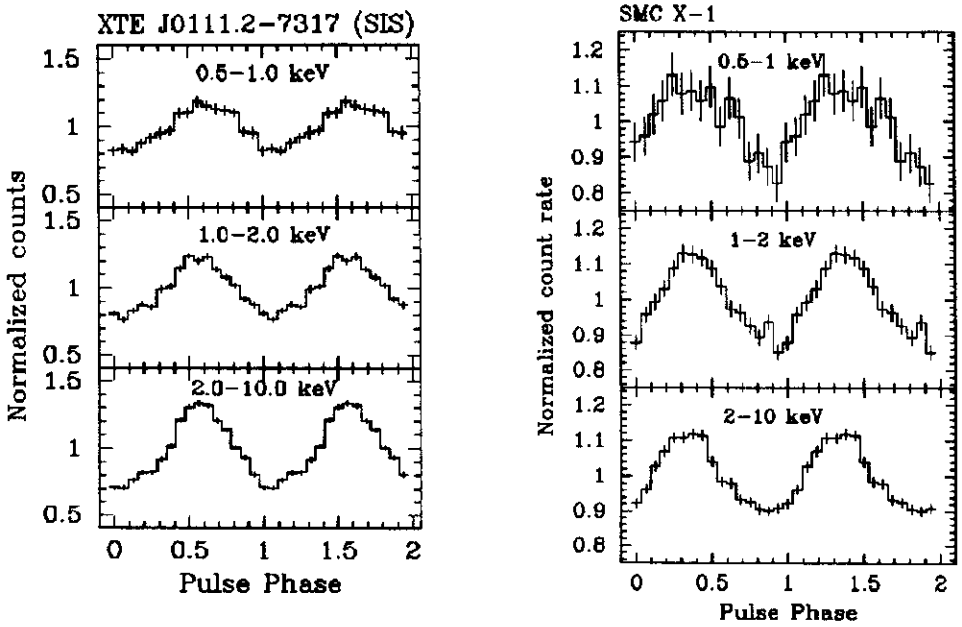

FIGURE 6. Pulse profiles of a Be transient XTE J0111.2−7313 and a massive X-ray binary pulsar SMC X-1 observed with ASCA.

Hence, it is likely that all the emission in 0.5-10 keV, including the soft excess emission, originate from the same site, for instance from accretion columns on the neutron star magnetic poles. The soft excess feature in spectra would be a feature intrisically common to X-ray pulsar emission from neutron star accretion columns, because many pulsars in all sub-class of X-ray pulsars exhibit such a feature.

ACKNOWLEDGEMENTS

The author thanks B. Paul for the useful comments and discussion.

REFERENCES

Angelini, L. et al. 1995, ApJ, 449, L41

Angelini, L. Church, M.J., Parmar, A.N., Balucinska-Church, M., Mineo, T. 1998, A&A, 339, L41

Bildsten, L., Chakrabarty, D., Chiu, J., et al. 1997, ApJS, 113, 367

Coe, M.J., 1999, in *The Evolution of Galaxies on Cosmological Time Scale*, ASP Conference Series, eds. J.E. Beckmann and T.J. Mahoney, in press.

Corbet R.H.D. 1986, MNRAS, 220,1047

Corbet R.H.D., Marshall, F.E., Peele, A.G, Takeshima, T. 1999, ApJ, 517, 956

Corbet R.H.D., Peele, A.G. 2000, ApJ, in press

Cowley, A.P., et al. 1997, PASP, 109, 21

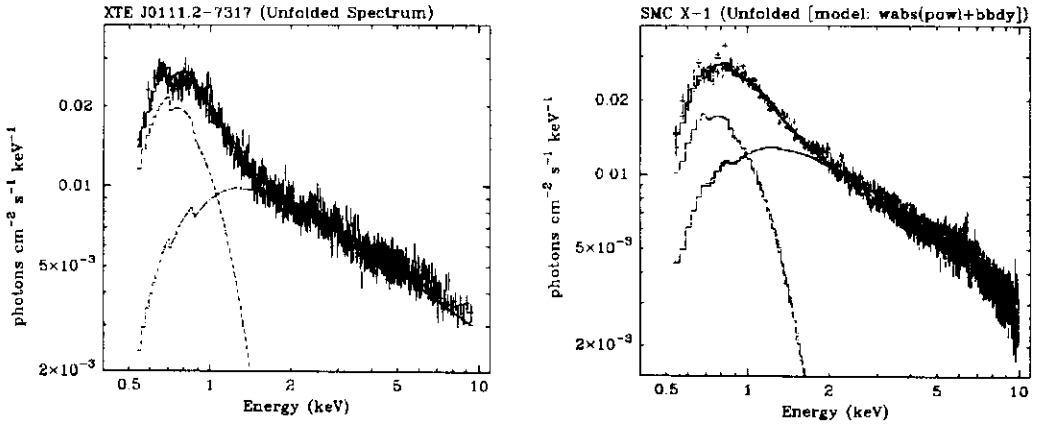

FIGURE 5. Energy spectra of a Be transient XTE J0111.2−7313 and a massive X-ray binary pulsar SMC X-1 observed with ASCA.

ples of such a soft excess feature were obtained from ASCA observations of TrXBPs in SMC, such as RX J0059.2−7138 (Hughes 1994, Kohno et al. 2000) and XTE J0111.2−7317 (Paul et al. 1999, Yokogawa et al. 2000b).

The energy spectrum with soft excess feature observed with ASCA from a TrXBP, XTE J0111.2−7317 is compared in Figure 6 with that observed with ASCA from a HMXB pulsar SMC X-1. Both can be fitted by a model of power law plus blackbody emission. The best fit parameters are $\Gamma = 0.8$, $kT = 0.15$ keV, and $N_{\rm H} = 2.7 \times 10^{21}$ cm^{-2}, and $\Gamma = 0.8$, $kT = 0.18$ keV, and $N_{\rm H} = 2.2 \times 10^{21}$ cm^{-2}, respectively for XTE J0111.2−7317 and SMC X-1. Thus, the spectral model that involves a power law and a soft blackbody emission, which is widely adopted to fit the soft-excess spectra observed from X-ray pulsars, can be adopted also to interprete the soft-excess feature seen in the spectra of some TrXBPs.

However, the total X-ray luminosities of these sources are 1.8×10^{38} erg s^{-1} and 2.4×10^{38} erg s^{-1}, respectively at the distance of SMC. If the soft excess emission is really blackbody, the luminosity fraction of the blackboly emission is about one thenth of the total luminosity. This requires blackbody radii of several hundred km if the surces are really located in the SMC.

The energy dependent pulse profiles of XTE J0111.2−7317 and SMC X-1 are shown in Figure 7. As can be seen, the pulse shape and pulse fraction do not change drastically with energies in these pulsars, although the pulse amplitude in XTE J0111.2−7317 changes slightly. This means that the soft excess component is pulsating in the same manner as the power law component. Thus the blackbody interpretation seems implausible, because the corresponding size of blackbody emission is several 10 times the neutron star radius at the distance of SMC and moreover this soft excess component should be pulsating.

RESULTS FROM X-RAY SURVEYS WITH ASCA

Yoshihiro Ueda

Institute of Space and Astronautical Science, Kanagawa 229-8510, Japan

ABSTRACT

We present main results from X-ray surveys performed with *ASCA*, focusing on the *ASCA* Large Sky Survey (LSS), the Lockman Hole deep survey, and the *ASCA* Medium Sensitivity Survey (AMSS or the GIS catalog project). The Log N - Log S relations, spectral properties of sources, and results of optical identification are summarized. We discuss implications of these results for the origin of the CXB.

KEYWORDS: diffuse radiation — surveys — galaxies: active — X-rays: galaxies

1. INTRODUCTION

Understanding the origin of the Cosmic X-ray Background (CXB or XRB) and cosmological evolution of X-ray extragalactic populations is one of the main goals of X-ray astronomy. In the soft X-ray band, the *ROSAT* satellite resolved 80% of the 0.5–2 keV CXB into individual sources (Hasinger *et al.* 1998) and optical identification revealed that the major population is type-I AGNs (Schmidt *et al.* 1998). Because of the technical difficulties, imaging sky surveys in the hard X-ray band (above 2 keV), where the bulk of the CXB energy arises, were not available until the launch of *ASCA*. The sensitivity limits achieved by previous mission such as *HEAO1* (Piccinotti *et al.* 1982) and *Ginga* (Kondo *et al.* 1991) are at most $\sim 10^{-11}$ erg s^{-1} cm^{-2} (2–10 keV), and the sources observed by them only account for 3% of the CXB intensity in the 2–10 keV band. In particular, there is a big puzzle on the CXB origin, called the "spectral paradox": bright AGNs observed with *HEAO1*, *EXOSAT* and *Ginga* have spectra with an average photon index of $\Gamma = 1.7-1.9$ (e.g., Williams *et al.* 1992), which is significantly softer than that of the CXB itself ($\Gamma \simeq 1.4$; e.g., Gendreau *et al.* 1995). Furthermore, the broad band properties of sources at fluxes from $\sim 10^{-11}$ to $\sim 10^{-13}$ erg s^{-1} cm^{-2} (2–10 keV) are somewhat puzzling according to previous studies. The extragalactic source counts in the soft band (0.3–3.5 keV) obtained by *Einstein* Extended Medium Sensitivity Survey (EMSS; Gioia *et al.* 1990) is about 2–3 times smaller than that in the hard band (2–10 keV) obtained by the *Ginga* fluctuation analysis (Butcher *et al.* 1997) when we assume a power-law photon index of 1.7.

The *ASCA* satellite (Tanaka, Inoue, & Holt 1994), launched in 1993 February, was expected to change this situation. It is the first imaging satellite capable of

TABLE 1. Summary of *ASCA* Surveys

Survey Project	Area (deg^2)	Sensitivity (2–10 keV) (erg s^{-1} cm^{-2})
Large Sky Survey (LSS)	7.0	1.5×10^{-13}
Deep Sky Survey (DSS)	0.3	4×10^{-14}
Lockman Hole Deep Survey	0.2	4×10^{-14}
Survey of deep *ROSAT* fields	1.0	5×10^{-14}
ASCA Medium-Sensitivity Survey (AMSS)	110	7×10^{-14}

study of the X-ray band above 2 keV with a sensitivity up to several 10^{-14}erg s^{-1} cm^{-2} (2–10 keV) and covers the wide energy band from 0.5 to 10 keV, which allows us to directly compare results of the energy bands below and above 2 keV with single detectors, hence accompanied with much less uncertainties than previous studies. By taking these advantages, several X-ray surveys have been performed with *ASCA* to reveal the nature of hard X-ray populations: the *ASCA* Large Sky Survey (LSS; Ueda *et al.* 1998), the *ASCA* Deep Sky Survey (DSS; Ogasaka *et al.* 1998; Ishisaki *et al.* 1999 for the Lockman Hole), the *ASCA* Medium-Sensitivity Survey (AMSS or the GIS catalog project: Ueda *et al.* 1997, Takahashi *et al.* 1998, Ueda *et al.* 1999b; see also Cagnoni, Della Ceca, & Maccacaro 1998 and Della Ceca *et al.* 1999), a survey of *ROSAT* deep fields (Georgantopoulos *et al.* 1997; Boyle *et al.* 1998), and so on. The sensitivity limits and survey area are summarized in Table 1. In this paper, we present main results of the *ASCA* surveys, focusing on the LSS (§ 2), the Lockman Hole deep survey (§ 3), and the AMSS (§ 4). In § 5, we summarize these results and discuss their implications for the origin of the CXB.

2. THE LARGE SKY SURVEY

2.1. X-ray Data

The survey field of the *ASCA* Large Sky Survey (LSS; Ueda *et al.*, 1998) is a continuous region near the north Galactic pole, centered at $RA(2000) = 13^h14^m$, $DEC(2000) = 31°30'$. Seventy-six pointings have been made over several periods from Dec. 1993 to Jul. 1995. The total sky area observed with the GIS and SIS amounts to 7.0 deg^2 and 5.4 deg^2 with the mean exposure time of 56 ksec (sum of GIS2 and GIS3) and 23 ksec (sum of SIS0 and SIS1), respectively. From independent surveys in the total (0.7–7 keV), hard (2–10 keV), and soft (0.7–2 keV) bands, 107 sources are detected with sensitivity limits of 6×10^{-14}, 1×10^{-13}, and 2×10^{-14} erg s^{-1} cm^{-2} , respectively. The Log N - Log S relations derived from the LSS are summarized in Ueda *et al.* (1999a) together with a complete X-ray source list. At these flux limits, 30(±3)% of the CXB in the 0.7–7 keV band and 23(±3)% in the 2–10 keV band have been resolved into discrete sources. The 2–10 keV Log N - Log S relation combined with the AMSS result (§4) is plotted in Figure 3.

The spectral properties of the LSS sources suggest that contribution of sources with hard energy spectra become significant at a flux of $\sim 10^{-13}$ erg s^{-1} cm^{-2} (2–10 keV), which are different from the major population in the soft band. The average 2–10 keV photon index is 1.49±0.10 (1σ statistical error in the mean value) for 36 sources detected in the 2–10 keV band with fluxes below 4×10^{-13} erg s^{-1} cm^{-2}, whereas it is 1.85±0.22 for 64 sources detected in the 0.7–2 keV band with fluxes below 3×10^{-13} erg s^{-1} cm^{-2}. The average spectrum of 74 sources detected in the 0.7–7 keV band with fluxes below 2×10^{-13} shows a photon index of 1.63±0.07 in the 0.7–10 keV range: this index is consistent with the comparison of source counts between the hard and the soft band.

To investigate the X-ray spectra of these hard sources, we made deep follow-up observations with *ASCA* for the five hardest sources in the LSS, selected by the apparent 0.7–10 keV photon index from the source list excluding very faint sources. The results are summarized in Ueda *et al.* (1999c); see also Sakano *et al.* (1998) and Akiyama *et al.* (1998) for AX J131501+3141, the hardest source in the LSS. Three sources in this sample are optically identified as narrow-line AGNs and one is a weak broad-line AGN by Akiyama *et al.* (2000); one is not identified yet. We found that spectra of these sources are most likely subject to intrinsic absorption at the source redshift with column densities of $N_{\rm H} = 10^{22} \sim 10^{23}$ cm^{-2}.

2.2. Optical Identification

Akiyama *et al.* (2000) summarize the results of optical identification for a subsample of the LSS sources, consisting of 34 sources detected in the 2–7 keV band with the SIS. The major advantage of this sample compared with other *ASCA* surveys is good position accuracy; it is 0.6 arcmin in 90% radius from the *ASCA* data alone, thanks to superior positional resolution of the SIS. To improve the position accuracy further, we made follow-up observations with *ROSAT* HRI over a part of the LSS field in Dec. 1997. Optical spectroscopic observations were made using the University of Hawaii 88″ telescope, the Calar Alto 3.5m telescope, and the Kitt Peak National Observatories Mayall 4m and 2.1m telescopes.

Out of the 34 sources, 30 are identified as AGNs, 2 are clusters of galaxies, 1 is a Galactic star, and only 1 object remains unidentified. The identification as AGNs is based on existence of a broad emission line or the line ratios of narrow emission lines ([NII]6583Å/Hα and/or [OIII]5007Å/Hβ); see Akiyama *et al.* 2000 and references therein. Figure 1(a) shows the correlation between the redshift and the apparent photon index in the 0.7–10 keV range, which is obtained from a spectral fit assuming no intrinsic absorption, for the identified objects. The 5 sources that have an apparent photon index smaller than 1.0 are identified as 4 narrow-line AGNs and 1 weak broad-line AGN, all are located at redshift smaller than 0.5. On the other hand, X-ray spectra of the other AGNs are consistent with those of nearby type 1 Seyfert galaxies. Four high redshift broad-line AGNs show somewhat apparently hard spectra with an apparent photon index of 1.3 ± 0.3, although it may be still marginal due to the limited statistics.

To avoid complexity in classifying the AGNs by the optical spectra, we divide the identified AGNs into two using the X-ray data: the "absorbed" AGNs which show intrinsic absorption with a column density of $N_{\rm H} > 10^{22}$ cm^{-2} and the "less-absorbed" AGNs with $N_{\rm H} < 10^{22}$. Correcting the *flux* sensitivity for different X-ray spectra, we found the contribution of the absorbed AGNs is almost comparable to that of less-absorbed AGNs in the 2–10 keV source counts at a flux limit of 2×10^{-13} erg s^{-1} cm^{-2}. Figure 1(b) shows the correlation between the redshift and the 2–10 keV luminosity of the identified AGNs. The redshift distribution of the 5 absorbed AGNs is concentrated at $z < 0.5$, which contrasts to the presence of 15 less-absorbed AGNs at $z > 0.5$. This suggests a deficiency of AGNs with column densities of $N_{\rm H} = 10^{22-23}$ at $z = 0.5$–2, or in the X-ray luminosity range larger than 10^{44} erg s^{-1}, or both. Note that if the 4 broad-line AGNs with hard spectra have intrinsic absorption instead of other hardening mechanism such as Compton reflection, it could complement this deficiency.

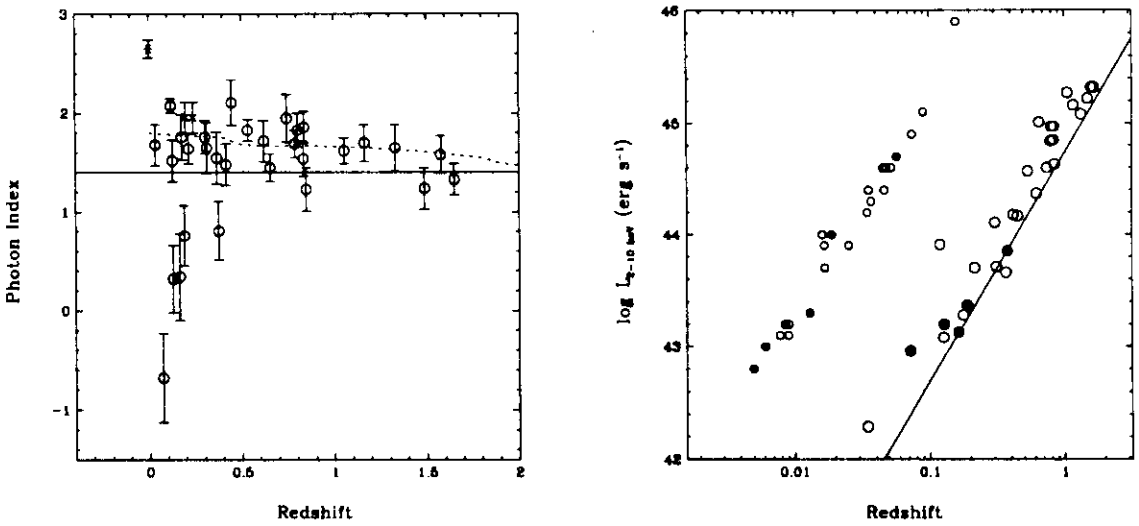

FIGURE 1. (a) left: the correlation between the redshift and the apparent 0.7–10 keV photon index for the identified objects in the LSS (Akiyama *et al.* 2000). The open circles, crosses, and asterisk represent AGNs, clusters of galaxies, and a Galactic star, respectively. The dotted curve shows the expected apparent photon index in the observed 0.7–10 keV band as a function of redshift, for a typical spectrum of type-1 Seyfert galaxies with a Compton reflection component. (b) right: The 2–10 keV luminosity versus redshift diagram for the LSS AGNs (with large open circles, Akiyama *et al.* 2000), and for the *HEAO1*A2 AGNs (with small marks, Piccinotti *et al.* 1982). The "absorbed" AGNs are plotted with dots. Lines indicate detection limits of the LSS for a source with an photon index of 1.7 with no intrinsic absorption.

3. THE LOCKMAN HOLE DEEP SURVEY

Deep surveys were performed with *ASCA* over several fields (Ogasaka *et al.* 1998), although optical identification is more difficult than the LSS because of faint flux levels and source confusion problem. To overcome this difficulty, we have been conducting a deep survey of the Lockman Hole, where the *ROSAT* deep survey was performed (Hasinger *et al.* 1998). The advantage of selecting this field is that we already have a complete soft X-ray source catalog down to a flux limit of 5.5×10^{-15} erg s^{-1} cm^{-2} (0.5–2 keV), most of which have been optically identified (Schmidt *et al.* 1998). In addition, we utilized an X-ray source list at even fainter flux limits (G. Hasinger, private communication). Since the flux limits of the *ROSAT* surveys are extremely low, we can expect most of *ASCA* sources could have *ROSAT* counterparts within reasonable range of spectral hardness. Utilizing positions of the *ROSAT* sources, we can determine the hard-band flux for individual sources, which would otherwise have been difficult to separate, to a flux limit of 3×10^{-14} erg s^{-1} cm^{-2} (2–10 keV). Preliminary results are reported in Ishisaki *et al.* (1999).

Up to present, we have made 3 pointings in the direction of the Lockman Hole with *ASCA* on 1993 May 22–23, 1997 April 29–30, and 1998 November 27 for a net exposure of 63 ksec (average of the 8 SIS chips), 64 ksec, and 62 ksec, respectively. The pointing positions were arranged so that the superposed image of the SIS field of views (FOVs) covers the PSPC and HRI FOVs as much as possible. We here used only the SIS data considering its superior positional resolution. Analysis was made through the 2-dimensional maximum-likelihood fitting to a raw, superposed image in photon counts space in the sky coordinates, with a model consisting of source peaks (point spread functions) and the background. As a first step, we put sources into the model at the positions of the *ROSAT* catalogs. Then, after checking the residual image of the fit, we added remaining peaks that were missing in the *ROSAT* catalogs. Thus, we determined the significance and flux of each source in three energy bands, 0.7–7 keV, 2–7 keV, and 0.7–2 keV, including new sources detected with *ASCA*. We corrected for the degradation of detection efficiency caused by the radiation damage using the CXB intensity. Note that the *ASCA* sensitivity limits strongly depends on position due to the multiple pointings and the vignetting of the XRT.

We detected 27 sources altogether with significances higher than 3.5σ in either of the three survey bands. Two sources were newly detected with *ASCA*. One object is a variable source having a 0.7–7 keV photon index of about 1.7, which was very faint during the *ROSAT* observations. The other shows a very hard spectrum and is detected only in the 2–7 keV band. In the combined SIS FOVs, 43 sources out of 50 sources in the Schmidt *et al.* (1998) catalog are located. Identification of *ASCA* sources using the *ROSAT* catalog is summarized in Table 2. Since the number of sources detected in the 2–7 keV band is limited due to poor photon statistics, we here use the results for 25 sources detected in the 0.7–7 keV band for comparison with the *ROSAT* survey. Four unidentified sources in the *ASCA* survey have *ROSAT* counterparts in the deeper X-ray source catalog (G. Hasinger, private

TABLE 2. Summary of optical identification of the *ASCA* Lockman Hole deep survey by the *ROSAT* catalog (Schmidt *et al.* 1998)

Population	*ROSAT*	*ASCA* (0.7–7 keV)
Total	43	25
Type-1 AGN (a-c)	26	13
Type-2 AGN (d-e)	7	6
Group/Galaxies	3	0
Star	3	1
Unidentified	4	4+1

communication) and remaining one is the variable source detected only with *ASCA*. For AGNs identified by Schmidt *et al.* (1998), we divided them into two according to their optical spectra: (1) type-1 AGNs, corresponding to either of class a, b, or c, showing broad emission lines, and (2) type-2 AGN, class d or e, showing only narrow emission lines. As noticed from the table, 6 out of 7 type-2 AGNs were detected, whereas only half of the 26 type-1 AGNs were detected with *ASCA*, which covers much harder band than the *ROSAT*. This suggests that contribution of type-2 AGNs are more dominant in higher energy bands than in the soft band at similar flux levels.

4. THE *ASCA* MEDIUM-SENSITIVITY SURVEY

Because these surveys are limited in sky coverage, the sample size is not sufficient to obtain a self-consistent picture about the evolution of the sources over the wide fluxes, from $\sim 10^{-11}$ erg s^{-1} cm^{-2} (2–10 keV) which is the sensitivity limit of *HEAO1* A2 (Piccinotti *et al.* 1982), down to $\sim 10^{-13}$ erg s^{-1} cm^{-2} (2–10 keV), that of *ASCA* . To complement these shortcomings, we have been working on the project called the "*ASCA* Medium Sensitivity Survey (AMSS)", or the GIS catalog project. In the project, we utilize the GIS data from the fields that have become publicly available to search for serendipitous sources. The large field of view and the low-background characteristics make the GIS instrument ideal for this purpose.

Main results from the AMSS are reported in Ueda *et al.* (1999b), which were obtained from selected GIS fields of $|b| > 20°$ observed from 1993 to 1996, covering the total sky area of 106 deg^{-2}. The sample contains 714 serendipitous sources, of which 696, 323, and 438 sources are detected in the 0.7–7 keV (total), 2–10 keV (hard), and 0.7–2 keV (soft) band, respectively. This is currently the largest X-ray sample covering the 0.7–10 keV band. Figure 2(a) shows the correlation between the 0.7–7 keV flux and the hardness ratio between the 2–10 keV and 0.7–2 keV count rates. We also plot the average hardness ratio in several flux ranges, separated by the dashed curves, with crosses. It is clearly seen that the average spectrum becomes harder with a decreasing flux: the corresponding photon index (assuming

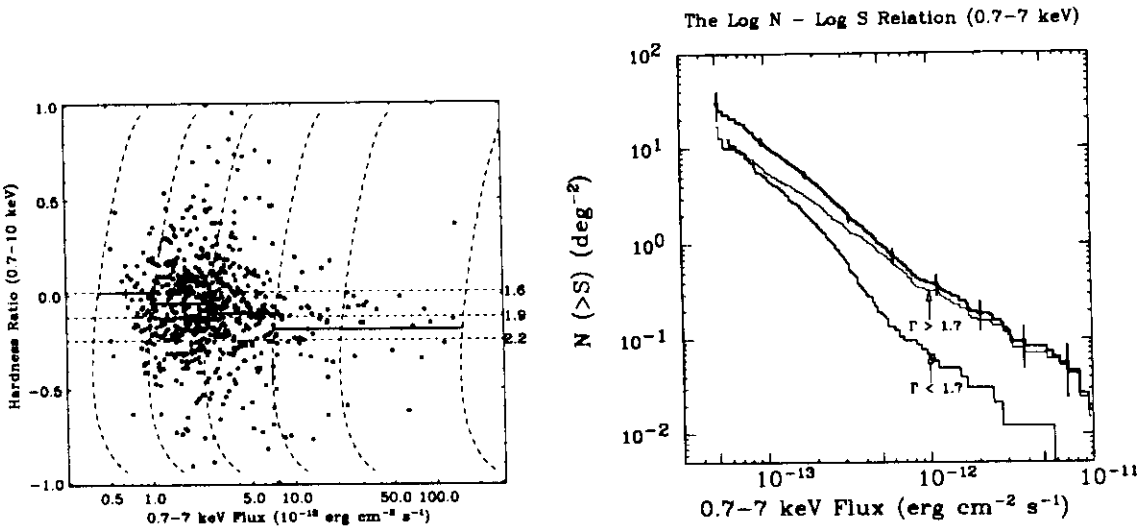

FIGURE 2. (a) left: The correlation between the 0.7–7 keV flux and the hardness ratio between the 0.7–2 keV and 2–10 keV count rates for sources detected in the 0.7–7 keV survey in the AMSS sample (Ueda *et al.* 1999b). The crosses show the average hardness ratios (with 1σ errors in the mean value) in the flux bin separated by the the dashed curves, at which the count rate hence the sensitivity limit is constant. The dotted lines represent the hardness ratios corresponding to a photon index of 1.6, 1.9, and 2.2 assuming a power law spectrum. (b) right: The integral Log N - Log S relations in the 0.7–7 keV survey band, derived from the AMSS sample. The medium-thickness curve represents the result for the hard source sample, consisting of sources with an apparent 0.7–10 keV photon index Γ smaller than 1.7, the thin curve represents that for the soft source sample (with Γ larger than 1.7), and the thick curve represents the sum. The 90% statistical errors in source counts are indicated by horizontal bars at several data points.

a power law over the 0.7–10 keV band with no absorption) changes from 2.1 at the flux of $\sim 10^{-11}$ erg s^{-1} cm^{-2} to 1.6 at $\sim 10^{-13}$ erg s^{-1} cm^{-2} (0.7–7 keV). Similar hardening are also reported in the 2–10 keV range by Della Ceca *et al.* (1999) using 60 serendipitous sources. Figure 2(b) shows the integral Log N - Log S relations in the 0.7–7 keV survey band for the soft source sample, consisting of sources with an apparent 0.7–10 keV photon index larger than 1.7, and for the hard source sample, with an index smaller than 1.7. This demonstrates that sources with hard energy spectra in the 0.7–10 keV range are rapidly increasing with decreasing fluxes, compared with softer sources.

5. SUMMARY

The *ASCA* surveys have brought a clear, self-consistent picture about statistical properties of sources that constitute about 30% of the CXB in the broad energy

band of 0.7–10 keV. Figure 3 summarizes the 2–10 keV Log N - Log S relation obtained from the *ASCA* surveys together with the results from previous missions. The direct source counts from combined results of the LSS (Ueda *et al.* 1999b) and the AMSS (Ueda *et al.* 1999c; these contain the data used by Cagnoni, Della Ceca, & Maccacaro 1998) give the tightest constraints so far over a wide flux range from $\sim 10^{-11}$ to $\sim 7 \times 10^{-14}$ erg s^{-1} cm^{-2}: $N(>S) = 16.8\pm7.2$ (90% statistical error), 11.43±2.4, 3.76±0.42, 1.08±0.17, and 0.33±0.09 deg^{-2}, at $S = 7.4 \times 10^{-14}$, 1.0×10^{-13}, 2.0×10^{-13}, 4.0×10^{-13}, and 1.0×10^{-12} erg s^{-1} cm^{-2}, respectively. The DSS gives a direct source counts at the faintest flux, 3.8×10^{-14} erg s^{-1} cm^{-2}(Ogasaka *et al.* 1998), whereas the fluctuation analysis of deep SIS fields constrains the Log N - Log S relation at fluxes down to 1.5×10^{-14} (Gendreau, Barcons, & Fabian 1998). As seen from the figure, the *ASCA* direct source counts smoothly connect the two regions constrained by the *Ginga* and *ASCA* fluctuation analysis.

The AMSS/LSS results demonstrate that the average spectrum of X-ray sources becomes harder toward fainter fluxes: the apparent photon index in the 0.7–10 keV range changes from 2.1 at the flux of $\sim 10^{-11}$ to 1.6 at $\sim 10^{-13}$ erg s^{-1} cm^{-2} (2–10 keV). This fact can be explained by the rapid emergence of population with hard energy spectra, as is clearly indicated in Figure 2(b). The evolution of broad-band properties of sources solves the puzzle of discrepancy discrepancy of the source counts between the soft (EMSS) and the hard band (*Ginga* and *HEAO1*). If we compare the *ASCA* Log N - Log S relations (including Galactic objects) between above and below 2 keV, the hard band source counts at $S \sim 10^{-13}$ erg s^{-1} cm^{-2} (2–10 keV) matches the soft band one when we assume a photon index of 1.6 for flux conversion, whereas at brighter level of $S = 4 \times 10^{-13} \sim 10^{-12}$ erg s^{-1} cm^{-2} (2–10 keV), we have to use a photon index of about 1.9 to make them match. The latter fact is consistent with the average 0.7–10 keV spectrum at the same flux levels, and can be connected the the "soft" spectrum of the fluctuation observed with *Ginga*, which shows a photon index of 1.8±0.1 in the 2–10 keV range (Butcher *et al.* 1997).

The optical identification revealed that the major population at fluxes of 10^{-13} erg s^{-1} cm^{-2} are AGNs. The population of hard sources, which are most responsible for making the average spectrum hard, are X-ray absorbed sources. They are mostly identified as narrow line (type-2) AGNs. The contribution of these type-2 AGNs is larger in the hard band than in the soft band at the same flux limit. Recent results of the 5–10 keV band survey by *BeppoSAX* confirms this tendency (Fiore *et al.* 1999). These results support the scenario that the CXB consists of unabsorbed AGNs and absorbed AGNs, whose contribution becomes more significant with decreasing fluxes and in harder energy band.

We found, however, possible evidence that is not consistent with the "unified scheme" of AGNs (e.g., Awaki *et al.* 1991), on which many AGN synthesis models are based. The LSS results may imply deficiency of X-ray luminous, absorbed AGNs, with $N_{\rm H} = 10^{22-23}$ at $z = 0.5$–2, or in the X-ray luminosity range larger than 10^{44} erg s^{-1}, although we cannot rule out possibility, for example, that there are many luminous AGNs at $z > 2$ with extreme heavy absorption of $N_{\rm H} > 10^{24}$. On the other hand, there is another implication that there could be a population of AGNs

at high redshifts ($z > 1$) that are optically identified as type-1 AGNs but have apparently hard X-ray spectra, although the origin of the hardness is not clear yet. Future surveys by *Chandra* and *XMM* together with optical identification of the AMSS sources will reveal the luminosity, number, and spectral evolutions of extragalactic populations including absorbed AGNs, which will eventually lead us to full understanding of the origin of the CXB.

ACKNOWLEDGEMENTS

I thank all the collaborators of our ASCA survey projects, especially, M. Akiyama, G. Hasinger, H. Inoue, Y. Ishisaki, I. Lehmann, K. Makishima, Y. Ogasaka, T. Ohashi, K. Ohta, M. Sakano, T. Takahashi, T. Tsuru, W. Voges, T. Yamada, and A. Yamashita.

REFERENCES

Akiyama, M., *et al.* 1998, ApJ, 500, 173
Akiyama, M., *et al.* 2000, ApJ, in press
Awaki, H., Koyama, K., Inoue, H., & Halpern, J.P. 1991, PASJ, 43, 195
Boyle , B.J., *et al.* 1998, MNRAS, 296, 1
Butcher, J.A., *et al.* 1997, MNRAS, 291, 437
Cagnoni, I., Della Ceca, R., & Maccacaro, T. 1998, ApJ, 493, 54
Della Ceca, R., *et al.* 1999, ApJ, 524, 674
Fiore, F., *et al.* 1999, MNRAS, 306, L55
Gendreau, K.C., *et al.* 1995, PASJ, 47, L5
Gendreau, K.C., Barcons, X., & Fabian, A.C. 1998, MNRAS, 297, 41
Georgantopoulos, I., *et al.* 1997, MNRAS, 291, 203
Gioia, I.M. *et al.* 1990, ApJS, 72, 567
Hasinger, G. 1998, AN, 319, 37
Hasinger, G., *et al.* 1998, A&A, 329, 482
Ishisaki, Y., *et al.* 1999, Advanced in Space Research, in press
Kondo, H. *et al.* 1982, in "Frontiers of X-ray Astronomy", Universal Academy Press, Tokyo, p.655
Ogasaka, Y., *et al.* 1998, Astro. Nachr., 319, 43
Piccinotti, G., *et al.* 1982, ApJ, 253, 485
Sakano, M. *et al.* 1998, ApJ, 505, 129
Schmidt, M., *et al.* 1998, A&A, 329, 495
Takahashi, T., Ueda, Y., Ishisaki, Y., Ohashi, T., & Makishima, K. 1998, AN, 319, 91
Tanaka, Y., Inoue, H., & Holt, S.S. 1994, PASJ, 46, L37
Ueda, Y., Takahashi, T., Ishisaki, Y., Makishima, K. & 1997, in "All-Sky X-Ray Observations in the Next Decade", RIKEN, Saitama, p55
Ueda, Y., *et al.* 1998, Nature, 391, 866
Ueda, Y., *et al.* 1999a, ApJ, 518, 656
Ueda, Y., Takahashi, T., Ishisaki, Y., Ohashi, T., & Makishima, K. 1999b, ApJ, 524, L11
Ueda, Y., *et al.* 1999c, Advanced in Space Research, in press
Williams, O.R. *et al.* 1992, ApJ, 389, 157

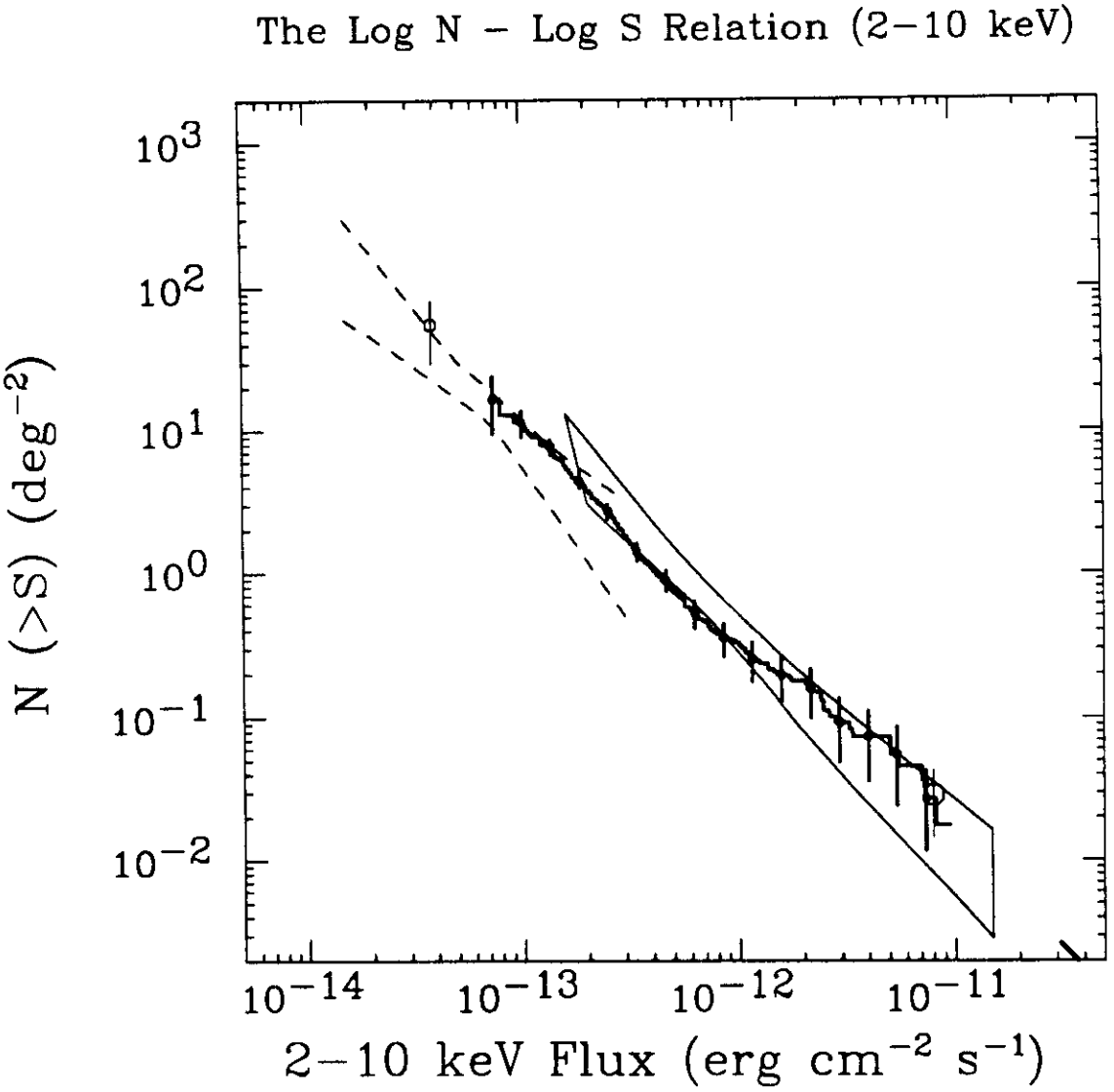

FIGURE 3. Summary of the 2–10 keV Log N - Log S relation obtained by the *ASCA* surveys, compared with previous results. The steps are the combined results from the LSS (Ueda *et al.* 1998) and the AMSS (Ueda *et al.* 1999b). The faintest point at 4×10^{-14} erg s^{-1} cm^{-2} is derived from the DSS utilizing the SIS data (Ogasaka *et al.* 1998). The trumpet shape between two dashed lines indicates 1σ error region from the fluctuation analysis of *ASCA* SIS deep fields (Gendreau, Barcons & Fabian 1998). The contour at $10^{-13} \sim 10^{-11}$ erg s^{-1} cm^{-2} represents the constraints by the *Ginga* fluctuation analysis at 90% confidence level (Butcher *et al.* 1997). The open circle at 8×10^{-12} erg s^{-1} cm^{-2} corresponds to the source count by *Ginga* survey (Kondo *et al.* 1991), and the thick-line above 3×10^{-11} erg s^{-1} cm^{-2} is the extragalactic Log N - Log S relation determined by *HEAO1* A2 (Piccinotti *et al.* 1982). All the horizontal bars represent 90% statistical errors in source counts.

DUST SCATTERED X-RAY HALO OF 4U 1538–52 OBSERVED WITH ASCA

F. Nagase [1], T. Dotani [1], T. Endo [1], H. Ozawa [1], S. Uno [2], T. Kotani [3], T. Mihara [4],

1) The Institute of Space and Astronautical Science, 3-1-1 Yoshinodai Sagamihara, Kanagawa 229-8510, Japan
2) Faculty of Social and Information Science, Nihon Fukushi University, 26-2 Higashihaemi-cho, Handa, Aichi 475-0012, Japan
3) Laboratory of High-Energy Astrophysics, NASA/GSFC, Greenbelt MD 20771, USA
4) The Institute of Physical and Chemical Research, 2-1 Hirosawa, Wako, Saitama 351-0198, Japan

ABSTRACT The eclipsing X-ray binary pulsar 4U 1538−522 was observed with ASCA in March 1994 throughout the eclipse transition. Evidence of extended X-ray halo due to scattering by interstellar dust grains was seen in both the X-ray image and spectrum obtained during the eclipse phase. The radial profiles obtained in 1-2 keV and 2-5 keV bands from 4U1538−52 are consistent with the previous results obtained with ROSAT and ASCA from other Galactic sources. The 1-10 keV spectrum during out-of-eclipse phase can be fitted by a simple power law model of photon index $\Gamma = 1.2$ with relatively large interstellar absorption column density. On the contrary, a steep continuum spectrum with a photon index of $\Gamma = 2.6$ was observed during the eclipse. Comparing the two spectra, we can estimate the column density of the dust grains toward the source, which is substantially less than the density of the astronomical interstellar grains. This support the idea that interstellar grains are "fluffy" aggregates of smaller solid particles.

KEYWORDS: eclipsing binaries; interstellar dust; X-ray pulsars; X-ray sources.

1. INTRODUCTION

The X-ray source, 4U 1538−52 is an eclipsing X-ray binary pulsar accreting mass from the massive companion star, QV Nor via stellar wind, with a binary period 3.73 d and a long pulse period of 530 s (e.g., Bildsten et al. 1997). From analysis of the Ginga X-ray spectra throughout an eclipse transition from ingress to egress, Clark et al. (1994) found the existence of a soft component that is superimposed on the power law spectrum at energies below 4.5 keV and they interpreted this component to be due to the scattering by interstellar dust grains. This X-ray binary pulsar, 4U 1538−52/QV Nor is a system similar to the X-ray pulsar Cen X-3 and the ASCA observation of Cen X-3 revealed dust scattering halo in the soft X-ray image observed during the eclipse phase (Woo et al. 1994). Motivated by the similarity of

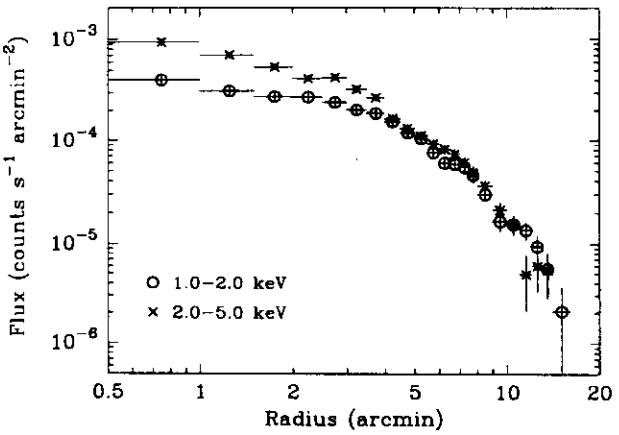

FIGURE 1. Radial profiles of the GIS images in the 1-2 keV and 2-5 keV bands observed with ASCA during the eclipse phase of 4U 1538−52. Background and contamination from the point source are subtracted.

the 4U 1538−52/QV Nor system to the Cen X-3 system, we observed 4U 1538−52 with ASCA (Tanaka et al. 1994) throughout the eclipse transition in March 1994 to search soft X-ray halo that might be produced by the interstellar dust-grain scattering.

2. IMAGE ANALYSIS

The image obtained with the ASCA SISs (Solid-state Imaging Spectrometer, i.e., CCD cameras) in the low energy band during an eclipse phase of 4U 1538−52 clearly shows the evidence of an extended halo. It was confirmed that the feature of halo extends over a radius of about 10 arcminutes, using the image of the GISs (Gas Imaging Spectrometer) which have a larger field of view of about 40 arcminutes diameter than that of SIS. The radial profiles of X-ray surface brightness derived from the GIS image taken during the eclipse phase of 4U 1538−5 show excess over the point spread function (PSF) for a point source in the energy ranges 1-2 keV and 2-5 keV.

Taking the results of spectral analysis together into account, we obtain the radial profile of dust scattering component after subtracting the residual contribution of the point source, contribution from a contamination source and the background. The resulting radial profiles of dust scattered component are shown in Figure 1 for 1-2 keV and 2-5 keV bands.

The radial profiles of the dust scattered halo observed from 4U 1538−52 in the 1-2 kev and 2-5 keV bands are relatively flat at small angular radius with turn over around 3-5 arcminutes. This feature is consistent with the previous ROSAT and ASCA observations for other Galactic sources (Predehl et al. 1991; Woo et al. 1994; Predehl & Schmitt 1995). In this analysis we for the first time derived the halo radial profile in the high energy band of 2-5 keV.

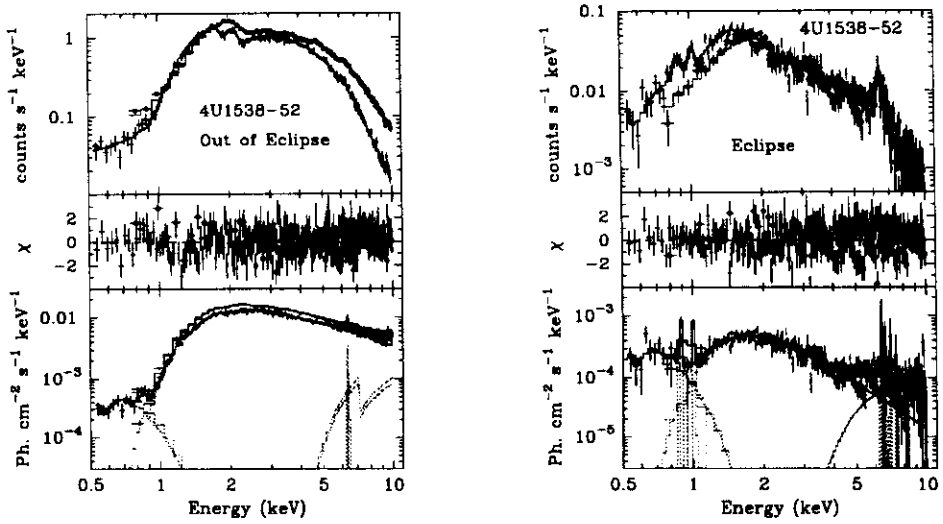

FIGURE 2. LEFT: Simultaneous fit to the GIS and SIS spectra observed from 4U 1538−52 during the out-of-eclipse phase: (top) observed counts spectra and the best fit model, (middle) residuals from the best-fit model, and (bottom) an unfolded spectrum derived from the best-fit parameters. RIGHT: Same as the left figures for the 4U 1538−52 eclipse phase spectrum.

3. SPECTRAL ANALYSIS

The energy spectrum of 4U 1538−52 is known by the feature of a hard power law with large soft X-ray absorption. The spectral feature changes gradually during the transition to eclipse along the ingress and egress, mainly due to soft X-ray absorption. Finally when the neutron star is totally eclipsed by the companion star, the direct beam from the neutron star surface disappears completely. During the eclipse of the neutron star, however, finite residual X-rays are visible with intensity of a few % of the direct beam because of scattering by the stellar wind in the binary system and interstellar dust grains. Spectra observed with ASCA during out-of-eclipse and during eclipse are shown in Figure 2 together with the best fit models and inferred incident spectra that are unfolded from the best-fit parameters.

The out-of eclipse spectrum in the left panel of Figure 2 shows that the direct pulsating component has a flat power law spectrum with soft X-ray absorption of $N_{\rm H} = 1.7 \times 10^{22}$ cm^{-2}. The eclipse spectrum in the right panel indicates that the extended component seen in the 1-5 keV image correspond to the steep power law spectrum with the soft X-ray absorption similar with the direct pulsating component. From the detailed analysis (see Nagase et al. 1999 for further details), the spectra of the direct beam and the dust scattered halo and their ratio in the 1-5

keV range are derived as follow:

$$F_{\rm direct}(E) = (7.58 \pm 0.21) \times 10^{-2} \times E^{-(1.25\pm0.02)},$$

$$F_{\rm dust}(E) = (0.52 \pm 0.15) \times 10^{-2} \times E^{-(2.6\pm0.2)},$$

$$R = \frac{F_{\rm dust}}{F_{\rm direct}} = (6.9 \pm 2.0) \times 10^{-2} \times E^{-(1.4\pm0.2)}.$$

This ratio shows an energy dependent dust scattering cross section integrated over the size of dust grains and the scattering angle. We compared this result with calculated energy dependence of dust scattering adopting the Rayleigh-Gans approximation (e.g., Mathis & Lee 1991; Smith & Dwek 1998). From this comparison, we obtained the amount of dust to be $M_{\rm dust} = (1.1 \pm 0.4) \times 10^{-5}$ g cm^{-2} assuming that the dust grains are made only from silicate. This value is substantially smaller than the dust column density $M_{\rm dust} = 4 \times 10^{-5}$ g cm^{-2} derived from the IRAS data on the assumption of $K = 40$ cm^2 g^{-1} (Hauser et al. 1984).

4. CONCLUSIONS

Results from present analysis of 4U 1538−52 data observed with ASCA are summarized as follow:
(1) We obtained radial profiles of dust scattered halo of 4U 1538−52 in both the low (1-2 keV) and medium (2-5 keV) energy bands.
(2) We derived the energy dependence of the dust scattering in the energy range of 1-5 keV.
(3) The column density of the dust grains derived from the present analysis is substantially less than the density estimated from the IRAS infrared observation.
(4) This supports the idea that interstellar grains are "fluffy" aggregates of smaller solid particles proposed by Mathis & Whiffen (1989).

REFERENCES

Bildsten, L., Chakrabarty, D., Chiu, J., et al. 1997, ApJS, 113, 367
Clark, G. W., Woo, J. W., Nagase, F. 1994, ApJ, 422, 336
Hauser, M. G. et al. 1984, ApJ, 285, 74
Mathis, J. S., Lee, C. -W. 1991, ApJ 376, 490
Mathis, J. S., Whiffen, G. 1989, ApJ, 341, 808
Nagase, F., et al. 1999, in preparation
Predehl, P., Bräuninger, H., Burkert, W., Schmitt, J. H. M. M. 1991, AAp, 246, L40
Predehl, P. Schmitt, J. H. M. M. 1995, AAp, 293, 889
Smith, R.K., Dwek, E. 1998, ApJ, 503, 831
Tanaka, Y., Inoue, H., Holt, S. S. 1994, PASJ, 46, L37
Woo, J. W., Clark, G. W., Day, C. S. R., Nagase, F., Takeshima, T. 1994, ApJ, 436, L5

DETECTION OF A PULSATING SOFT COMPONENT IN THE X-RAY PULSAR XTE J0111.2–7317

B. Paul[1,5], J. Yokogawa[2], M. Ozaki[1], F. Nagase[1], D. Chakrabarty[3], T. Takeshima[4] and G. W. Clark[3]

1) ISAS, 3-1-1 Yoshinodai, Sagamihara, Kanagawa 229-8510, Japan
2) Department of Physics, Kyoto University, Sakyo-ku, Kyoto 606-8502, Japan
3) Dept. of physics and Center for Space Research, MIT, Cambridge, MA 02139, USA
4) LHEA, NASA, Goddard Space Flight Center, Greenbelt, MD 20771
5) TIFR, Homi Bhabha Road, Mumbai 400005, India

ABSTRACT The newly discovered transient X-ray pulsar XTE J0111.2–7317 was observed with *ASCA* in its bright phase. The pulsation was found to be nearly sinusoidal with some energy dependence (17%, 21% and 30% pulse fractions in 0.5–1.0, 1.0–2.0 and 2.0–10.0 keV bands respectively). In addition to a hard power-law component in the 2–10 keV band, the energy spectrum has a soft excess in the 0.5–2 keV band. Thermal models for the soft excess require very large emission zone for the soft component and can be ruled out based on the pulsations observed at low energies. The low energy excess can however be accommodated if the incident spectrum is modeled as an inversely broken power-law with line of sight absorption. We have also detected an iron K_α emission line with equivalent width of 50 ± 14 eV.

KEYWORDS: binaries: general — pulsars: individual (XTE J0111.2–7317) – X-rays: stars

1. INTRODUCTION

The transient X-ray pulsar XTE J0111.2–7317 was discovered with the Proportional Counter Array (PCA) of the *Rossi X-ray Timing Explorer (RXTE)* in 1998 November (Chakrabarty et al. 1998a) and was simultaneously detected in hard X-rays (Wilson & Finger 1998) with the Burst and Transient Source Experiment (BATSE) onboard the *Compton Gamma Ray Observatory (CGRO)*. Initial BATSE observations also found the pulsar to be spinning-up with a very short time scale of $\left(\frac{P}{\dot{P}}\right) \sim$ 20 yr which is also a confirmation that the compact object is a neutron star. The pulsed X-ray luminosity in the hard X-ray band of BATSE is also high, and shows a positive correlation with the spin-up rate. Its association with the Small Magellanic Cloud indicates a large distance and very high luminosity, in excess of 10^{38} erg s^{-1} in the 2.0–10.0 keV band during the transient phase. A B type star with strong emission lines has been detected in the X-ray error box and this is likely to be the optical counterpart of this object (Israel et al. 1999). Following its discovery, a

Target of Opportunity observation was made during 1998 November 18–19 with the two imaging spectroscopic instruments SIS and GIS onboard the *Advanced Satellite for Cosmology and Astrophysics (ASCA)* and the position of the X-ray source was determined precisely (Chakrabarty et al. 1998b). The *ASCA* observation of the source was made to study the pulsations and the soft X-ray spectrum extending upto 10 keV.

2. TIMING AND SPECTRAL ANALYSIS

To study the temporal properties, we used light curves from the two GIS detectors with 0.5 s time resolution. The arrival times of the photons were corrected to the solar system barycenter. Data from the two detectors were added and power spectrum was generated. Pulsations were detected unambiguously with a period of 30.9497 ± 0.0004 s. The pulse profile is predominantly sinusoidal with indication of one small additional peak. To see the pulsations at low energy we have also generated pulse profiles in three different energy bands of 0.5–1.0, 1.0–2.0 and 2.0–10.0 keV from the barycentered SIS light curve. The normalized pulse profiles obtained from the SIS light curves in different energy bands are plotted in the left panel of figure 1. Slight difference in shape and larger modulation at higher energy are evident from these pulse profiles. A smaller pulse fraction at lower energy suggests spectral hardening during the pulse peak. The pulse fraction, defined as the ratio of the pulsed emission to the total emission was found to be 17%, 21% and 30% in the three energy bands of 0.5–1.0, 1.0–2.0 and 2.0–10.0 keV respectively. The pulse fraction is found to be nearly constant (~30%) in the entire 2.0–10.0 keV range.

The energy ranges chosen for spectral fitting are 0.55–10.0 keV for the SIS and 0.7–10.0 keV for the GIS. A simple power-law model with neutral absorber was found to be inadequate to represent the spectrum well, residual to the model fit showed presence of soft excess and indication of an emission line around 6.4 keV. A black-body component and an emission line component were added to the model which improved the fit considerably with power-law photon index 0.77 ± 0.02 and black-body temperature 0.148 ± 0.004 keV. If the soft component is assumed to be isotropic black-body emission from a spherical surface, the corresponding radius is estimated to be > 800 km, which is much larger than the neutron star surface area. The soft component could also be fitted to a thermal bremsstrahlung model of temperature 0.25 keV, but the emission measure is very high ($> 10^{62}$ cm^{-3}). In these spectral models in which a thermal component is assumed for the soft excess, the power-law contributes to only about 30% of the emission below 1.0 keV. The pulse fractions in the low and high energy bands of 0.5–1.0 keV and 2.0–10.0 keV are 17% and 30% respectively. Though the pulse fraction is smaller at lower energies, a pulsating nature of the soft component is evident. But, if the soft component is of thermal nature, as it requires a very large emission region the pulsations of this component remains unexplained. We therefore reject a thermal nature for the soft excess.

We found that the soft excess could be satisfactorily explained if we model the

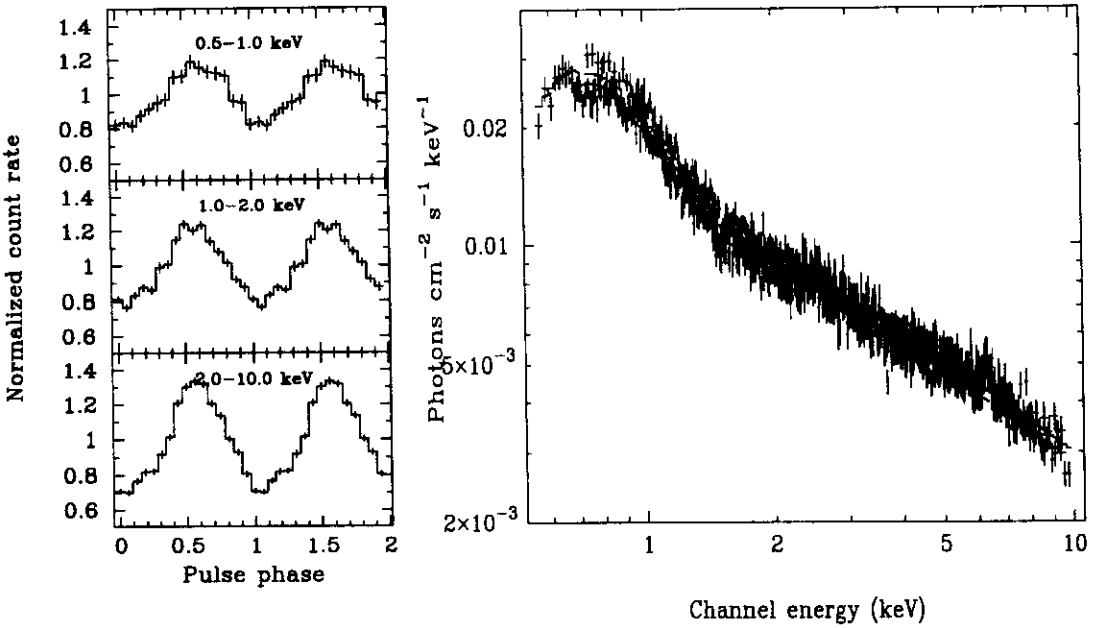

FIGURE 1. Background subtracted pulse profiles of XTE J0111.2–7317 in different energy bands obtained from the SIS light curves are shown on the left panel. The best fitted incident spectrum and the observed spectra (SIS and GIS) deconvolved through the detector response matrices are shown on the right.

entire spectrum as an inversely broken power-law with iron K_α emission line at 6.4 keV and line of sight absorption. For details about the spectral analysis including pulse phase resolved spectroscopy please refer to Yokogawa et al. (1999).

The best fitted incident spectrum is shown on the right hand side figure 1 along with the observed SIS and GIS spectra deconvolved through the detector response matrices. The observed X-ray flux in the 0.7–10.0 keV band is 3.6×10^{-10} erg s^{-1} cm^{-2}, which for an assumed distance of 65 kpc for this pulsar in the SMC and isotropic emission indicates an intrinsic luminosity of 1.8×10^{38} erg s^{-1}. The model spectrum described above has the following form

$$N(E) = IE^{-\Gamma_1} e^{-\sigma N_H} \text{ for } E < E_c \text{ and}$$

$$N(E) = IE_c^{(\Gamma_2-\Gamma_1)} E^{-\Gamma_2} e^{-\sigma N_H} \text{ for } E > E_c$$

where I is a normalization factor in units of photons cm^{-2} s^{-1} keV^{-1} at 1 keV.

The parameters for the inversely broken power-law model are :

$$N_H = 1.8 \pm 0.3 \times 10^{21} \text{ atoms cm}^{-2},$$
$$\Gamma_1 = 2.3 \pm 0.2,$$
$$E_c = 1.53 \pm 0.02 \text{ keV, and}$$
$$\Gamma_2 = 0.76 \pm 0.02.$$

The equivalent width of the iron emission line at 6.4 keV is 50 $\pm$ 14 eV.

3. DISCUSSION

The binary X-ray pulsars which are away from the galactic plane and therefore experience less interstellar absorption, show the presence of a soft component in the spectrum which is often described as a black-body and/or thermal bremsstrahlung emission (SMC X-1, Woo et al. 1995, Wojdowski et al. 1998; LMC X-4, Woo et al. 1996; 4U 1626–67, Orlandini et al. 1998). A thermal component for the soft part of the spectrum of 4U 1626–67 requires the size of emission region to be comparable to that of the neutron star, because the intrinsic luminosity of this source is of the order of 10^{35} erg s^{-1}. But for the pulsars in the Magellanic Clouds for which the distance is of the order of 60 kpc (and the luminosity is close to the Eddington value), a soft component dominating in the lower energy part of the spectrum will require an emission region which is a few orders of magnitude larger than the size of the neutron star. The bremsstrahlung component in LMC X-4, which is dominant in the intermediate energy range of 0.5–1.5 keV is also found to be pulsating (Woo et al. 1996). The pulsating nature of the soft component in XTE J0111.2–7317 and LMC X-4, which is also true for SMC X-1 is difficult to explain if a thermal origin is assumed for the low energy part of the spectrum. A two component power-law with different absorptions can instead explain the pulsations at low energy. A soft power-law component may also be a common feature of the binary X-ray pulsars, which is difficult to observe because most of the sources are in the galactic plane and experience large interstellar absorption.

The exact nature of this system in unknown but a possible optical counterpart has been identified which is a Be-type star (Israel et al. 1999). The characteristics of this pulsar, like its transient nature, hard X-ray spectrum and high X-ray luminosity are analogous to the pulsars in binary systems with high mass companion. A pulse period of 31 s is also much larger than the period of X-ray pulsars in low mass binaries. The rapid spin-up property during the transient phase is similar to the X-ray pulsars with high mass type companions (2S 1417–624 etc., Bildsten et al. 1997). The present outburst is analogous to the giant outbursts seen in Be X-ray pulsars characterized by high luminosity and high spin-up rates.

REFERENCES

Bildsten, L., et al. 1997, ApJS, 113, 367

Chakrabarty, D., et al. 1998a, IAU Circ., No. 7048

Chakrabarty, D., et al. 1998b, IAU Circ., No. 7062

Israel, G. L., et al. 1999, IAU Circ., No. 7101

Orlandini, M., et al. 1998, ApJ, 500, L163

Wilson, C. A., & Finger, M. H. 1998, IAU Circ., No. 7048

Wojdowski, P., et al. 1998, ApJ, 502, 253

Woo, J. W., et al. 1995, ApJ, 445, 896

Woo, J. W., et al. 1996, ApJ, 467, 811

Yokogawa, J., et al. 1999, ApJ (submitted)

SHORT-TERM SPECTRAL VARIATIONS DURING X-RAY FLARES IN BLACK HOLE CANDIDATES AND AGNS

Hitoshi Negoro

RIKEN, Cosmic Radiation Lab., 2-1 Hirosawa, Wako 351-0198, Japan

ABSTRACT

It has been pointed out that stellar black hole candidates (BHCs) and AGNs, especially Seyfert galaxies, have similar properties in X-ray time variations and energy spectra. We, however, have no crucial evidence that physical processes of these properties are the same. Here, is presented another common feature; spectral hardening during X-ray flares in these objects. Ginga data have revealed that X-ray "shots" in BHCs in the hard state have softer energy spectra then average spectra, and the spectra suddenly harden after the peak intensities of the shots. Using ASCA data of two Seyfert galaxies, MCG-6-30-15 and NGC 7314, it has been also found that spectra during bright "flares" are soft and become harder as the flares progress. The time variations in BHCs can be well explained by density fluctuations on the optical thin branch of an ADAF. The obtained similarity in the spectral evolution during the X-ray shots/flares and luminosity of these AGNs imply that the time variations in AGNs come from density fluctuations on the optical thick branch of an ADAF.

KEYWORDS: black hole candidates, Seyfert galaxies, time variations, Ginga, ASCA

1. INTRODUCTION

Stellar black hole candidates (BHCs) such as Cyg X-1 and AGNs, especially Seyfert galaxies, have the following common features:

- Rapid and chaotic time variations, characterized by a power-law PSD with a few knees (Miyamoto et al. 1991/ McHardy 1989).
- Energy spectra described by a power-law with a cutoff around 50-100 keV (Gierliński et al. 1997/ Zdziarski et al. 1995).
- Excess components from the power-law energy spectra below 2 keV (Balusińska et al. 1991/Turner et al. 1989).
- Soft energy spectra during X-ray flares (Negoro et al. 1994/ Matsuoka et al. 1990).

ASCA observations, however, show that only Seyfert galaxies exhibit relativistically skewed iron-lines with the centroid energy of 6.4 keV and an equivalent width

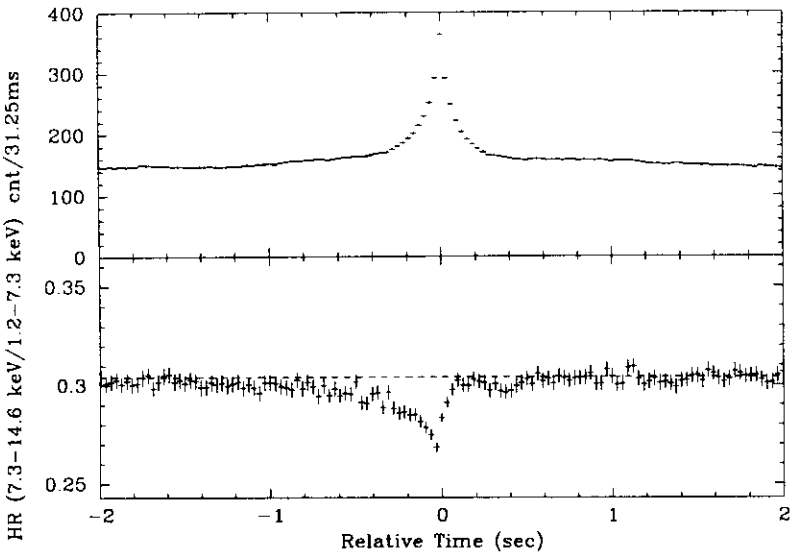

FIGURE 1. An average shot profile of Cyg X-1 in 1990 and hardness rations. The dashed line in the lower panel indicates the average ratio of all the X-rays (Negoro 1995).

of more than 100 eV, implying that a cold disk extends to the innermost radius (c.f., Matt et al. 1993). These naturally give rise to a question: are X-ray radiation processes and the origin of the time variations of these objects the same ? Here, another crucial similarity in spectral evolution during X-ray flares will be shown.

2. SPECTRAL CHANGES DURING FLARES

2.1. Stellar Black Hole Candidates

A superposition technique applied to Ginga data has revealed that shots of the BHCs in the hard state commonly have soft energy spectra, and that the spectra suddenly harden at the peak intensities of the shots, followed by complex changes (Fig. 1; Negoro et al. 1994; Negoro 1998). Time scales of the shots are about 0.1–0.2 s (FVWM), but the shots last more than 2-3 sec before and after the peaks. In RXTE data, similar properties have been found not only in a hard state but also in other states (Focke 1998; Feng et al. 1999).

2.2. Fourier Analyses

These properties in the superposed shots are consistent with structures in PSDs and phase lags below a few Hz (Negoro 1995). These results completely exclude a number of theoretical models based on a simple Comptonization process (Negoro 1995; also see Nowak 1999). The structures seen in PSDs and phase lags are mixtures of at least two components, two radiative processes (Negoro 1995).

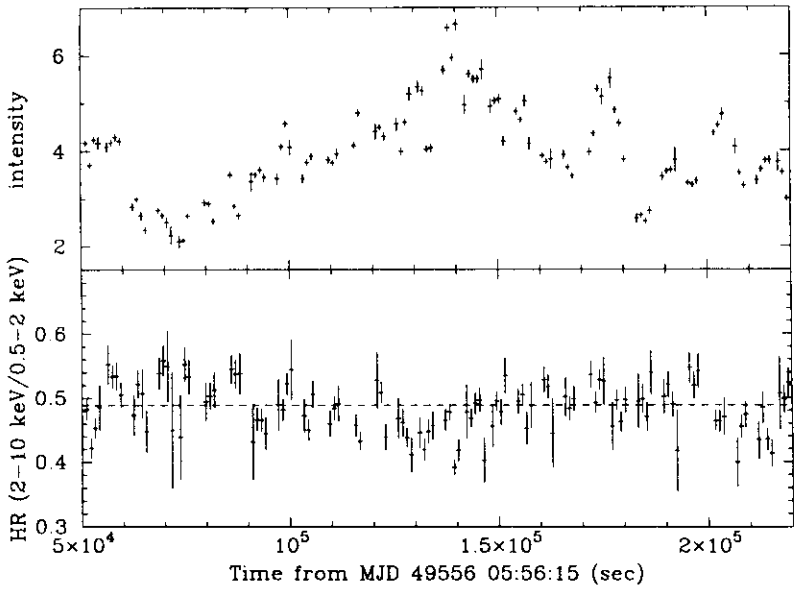

FIGURE 2. Light curve and hardness ratios of MCG-6-30-15. The dashed line in the lower panel indicates the average ratio.

2.3. Active Galactic Nuclei

ASCA observed a bright Seyfert galaxy MCG-6-30-15 in 1994, and detected a bright flare lasting for about 50 ksec (Iwasawa et al. 1996). An energy spectrum during the flare was confirmed to be softer than the average spectrum of all the data as previously shown. Furthermore, we have found that the spectrum becomes harder as the flare progresses (Fig. 3; Negoro et al. 1999).

A bright flare was also observed in NGC 7314 (Yaqoob et al. 1996). Preliminary results showed that a tendency similar to MCG-6-30-15 was recognized. The spectrum is the softest in the rise phase, and becomes harder. The hardest spectrum is obtained after the flare. Due to poor count statistics, a spectral change near the peak intensity is not clear. Detailed results about these Seyfert galaxies will be reported elsewhere (Negoro et al. 1999).

3. DISCUSSION

The mass of a central black-hole, the origin of the time variations and an iron-line profile are closely related. If the iron-line profiles really reflect the relativistic effect as observed with ASCA, an optically thick disk would extend to the innermost radius. The observed iron-lines with the centroid energy of 6.4 keV further constrain physical environment of the accretion disk.

If an external X-ray source illuminates the disk as usually assumed, luminosity should be below 1/10 of the Eddinton luminosity (e.g., Matt et al. 1993). In this case, the mass of black holes in these Seyferts can be estimated to be more than

10^6 $M_\odot$ from observed X-ray luminosities of $\sim 10^{43}$ erg/s. If the flares observed originate from hot spots rotating at small ($< 20\ r_g$) radii, the black holes would be further massive, say 10^8 $M_\odot$ (Iwasawa et al. 1996). In this case, however, the spectrum during the flares is expected to be almost time symmetric, and spectral hardening such as observed is not expected.

As shown before, the spectral hardening observed in the two Seyferts is similar to that in X-ray shots of BHCs, suggesting that the bright flares have the same origin with the X-ray shots, aperiodic mass accretion (Negoro 1995; Manmoto et al. 1996). The time scale of the shots, $\tau_{shot} = 0.1$–0.2 sec, is more than 100 times longer than the dynamical time scale in an accretion disk of a BH with 10 $M_\odot$. Thus, if the origin is the same, the black-hole mass of these Seyferts can be estimated to be $\sim (M_{BHC} \times (\tau_{flare}/\tau_{shot}) =) 10^6 M_\odot$.

Such small mass and the luminosities indicate $L/L_{Edd} \sim 0.1$–1, where the disks are likely to be on the optically thick branch of an ADAF. This conflicts with the above discussion about the 6.4 keV iron-lines. One possibility to avoid this conflict is that narrow cores of the observed iron-lines come from outer regions of accretion disks. Astro-E XRS observations will completely give us an answer to this question.

ACKNOWLEDGEMENTS

This work was partially supported by the special postdoctoral researchers program of RIKEN.

REFERENCES

Balucińska, M. & Hasinger, G. 1991, A&A, 241, 439

Fabian A., Rees, M., Stella, L. & White, N. 1989, MNRAS, 238, 729

Feng, Y, Li, T. & Chen, l. 1999, ApJ, 514, 373

Focke, W., 1998, Doctral thesis Univ. of Maryland; LHEA, GSFC/NASA

Gierliński, M., et al. 1997, MNRAS, 288, 958

Iwasawa, K. et al. MNRAS, 282, 1038

Manmoto, T., Takeuchi, M., Mineshige, S., Matsumoto, R., and Negoro. H. 1996, ApJ, 464, L135

Matsuoka, M., Piro, L., Yamauchi, M. & Murakami, Y. 1990, ApJ, 361, 440

Matt, G., Fabian, A. & Ross, R. 1993, MNRAS, 262, 179

McHardy, I., 1989, in Proc. 23rd ESLAB Symposium, ed. J. Hunt & B. Battrick, Vol. 1, 1111

Miyamoto, S., Kitamoto, S., Iga, S., Negoro, H. & Terada, K., 1991, ApJ, 383, 784

Negoro, H., Miyamoto, S. & Kitamoto, S. 1994, ApJ, 423, L127

Negoro, H., 1995, Doctral thesis Osaka Univ.; ISAS Research Note, 616

Negoro, H., 1998, Nuclear Physiscs B (Proc Suppl.), 69/1–3, 344

Negoro, H. et al, 1999, (in preparation)

Nowak, M. 1999, (in this voluume)

Zdziarsky, A., et al. 1995, ApJ, 438, L63

Turner, T.& Pounds, K. 1989, MNRAS, 240, 833

Yaqoob, T., Serlenmitsos, P., Turner, T., George, I. & Nandra, K., 1996, ApJ, 470, 27

THE POPULATION OF FAINT X-RAY SOURCES IN THE GALAXY AND THEIR CONTRIBUTION TO THE GALACTIC RIDGE X-RAY EMISSION

M. Sugizaki[1] [2], K. Matsuzaki[2], H. Kaneda[2], S. Yamauchi[3], K. Mitsuda[2], and ASCA Galactic Plane Survey team

1) National Space Develop Agency of Japan, 2-1-1, Sengen, Tsukuba, 305-8505, Japan
2) ISAS, 3-7-1, Yoshinodai, Sagamihara, 229-8510, Japan
3) Facility of Humanities and Social Sciences, Iwate University, 3-18-34, Ueda, Morioka, 020-8550, Japan

ABSTRACT

The Galactic ridge X-ray emission (GRXE) is an enhanced X-ray emission along the Galactic plane, whose origin still remains unknown. The GRXE was studied for the first time in the energy band of 0.5–10 keV with a spatial resolution of $3'$ by the ASCA Galactic plane survey which covers the spatial area of $|l| \lesssim 45^\circ$ and $|b| \lesssim 0.4^\circ$ almost uniformly. We determined the large scale distribution of the GRXE after eliminating discrete X-ray sources with a flux above $10^{-12.5}$ ergs cm^{-2} s^{-1} and revealed that the volume emissivity of the GRXE are highly concentrated within the 4 kpc arm. We resolved 163 discrete X-ray sources by imaging analysis and obtained the LogN-LogS relations of those sources. In the hard (2–10 keV) band, the slope of the LogN-LogS relation is significantly smaller than 1. Considering a scale height of the Galactic plane covered by the ASCA Galactic plane survey, we conclude that the slope of the LogN-LogS relation represents that the spatial distribution of the sources has a scale height as small as $\sim$10 pc, that the sources are distributed in arm-like structures, and/or that the relation reflects the luminosity function rather than the spatial distribution. We analyzed small-scale spatial intensity fluctuation of the GRXE after subtracting the large scale variations and the contributions of resolved discrete sources. The residual small-scale fluctuation is found to remain significantly over the photon-counting Poisson fluctuation. However, in the 2–10 keV band, the amplitude can be explained by the fluctuation of the cosmic X-ray background coming through the Galactic interstellar medium. From this, we can obtain a strong constraint to a flux and a number density of discrete sources if we are to explain the GRXE with a sum of discrete sources; more than 10^7 sources with the luminosity smaller than 10^{31}ergs s^{-1} must exist in the Galaxy. This source number density is larger by three orders of magnitude than that of CVs in the solar neighborhood, which would be a plausible candidate for the discrete source origin. Thus, We conclude that the diffuse emission origin should be much more probable even if it has large problems.

KEYWORDS: diffuse radiation — Galaxy: structure – X-rays: sources

1. INTRODUCTION

The Galactic ridge X-ray emission(hereafter GRXE) is an unresolved enhanced X-ray emission along the Galactic plane. The existence of the GRXE has been known from the early stage of the X-ray astronomy, however the origin still remains unknown (e.g. Warwick et al. 1985). The X-ray spectrum shows that originated from hot plasma with a temperature of 10^8K (e.g. Kaneda et al. 1997). If such a hot plasma is freely floated on the Galactic plane, it cannot be constrained by the gravitational potential in the Galaxy. An alternative possible hypothesis for the origin of the GRXE is a superposition of unresolved faint sources in the Galaxy. However, the population of faint X-ray sources in the Galaxy has not been measured in the X-ray band above 2 keV, because a high sensitive imaging observation in the higher energy X-ray band has been very difficult. ASCA with a moderate spatial resolution of $3'$ in the wide energy band of 0.5–10 keV, give a first opportunity to answer this problem. Then, we performed large area survey on the Galactic plane by ASCA and analyzed those image data.

2. ANALYSIS

The ASCA Galactic plane survey, which covers the area of $|l| \lesssim 45°$ and $|b| \lesssim 0.4°$ by 170 successive pointing observations each with a exposure time of $\sim$ 10 ks, was carried out from March, 1995 to April, 1999. We utilized data of the GIS for the image analysis, which prefer to the SIS in the points of a larger field of view (FOV) and a better calibration accuracy of the response function. We analyzed the large data of the ASCA Galactic plane survey by following steps:

(1) determine the large scale intensity variation averaged over each pointing,
(2) extract discrete X-ray sources,
(3) evaluate a small scale fluctuation of the unresolved residual emission

Since the image response of the ASCA is too complicated to deconvolve an original sky image, we applied an image fitting method. Also, we eliminated data of pointings contaminated by stray lights coming from bright X-ray sources outside of the FOV.

First, we determine the large-scale intensity variation. It is performed by fitting the image response for a uniform surface brightness to raw data in each GIS FOV. The derived large-scale intensity variation are shown in figure 1 for the soft (0.7–2 keV) and the hard (2–10 keV) band, respectively. The profile of the 2–10 keV band which have an excess within the area of $l \lesssim 35°$ corresponding to the 4-kpc arm, is consistent with those of the past observations (e.g. Warwick et al. 1985).

Next, we made a source survey. The procedure of the source survey is owed to that developed in the ASCA LSS (Ueda et al. 1999). We search for peaks of the image at the first and construct the model of the observed image, which consists of the large scale intensity variation and the extracted peaks. We recognized the peaks with a significance above 4σ in the image fitting as discrete X-ray sources. The source flux and the area surveyed for an arbitrary flux are estimated from the best fit model. We performed the source survey in the soft (0.7–2 keV) and the hard (2–10 keV) band individually and detected total 163 sources with a flux

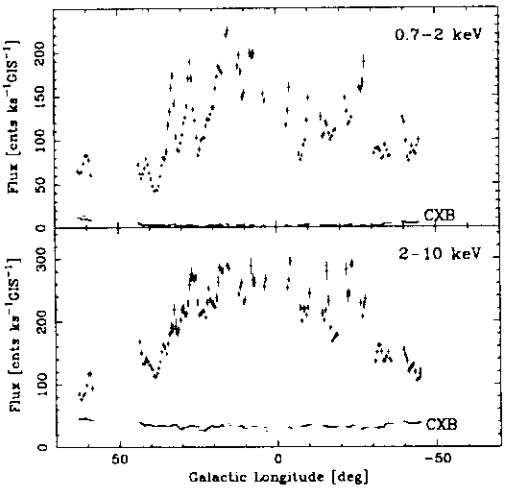

FIGURE 1. The large scale intensity variation of the GRXE averaged over each FOV of the GIS in the 0.7–2 keV band (upper) and the 2–10 keV band (lower). Contributions of the resolved discrete X-ray sources are eliminated. Inclusive contributions of the extragalactic cosmic X-ray background (CXB) coming through the Galactic ISM are shown together, which are calculated from the average spectrum of the CXB and the Galactic hydrogen column density obtained from the HI and CO line intensity.

down to $10^{-12.5}$ ergs cm^{-2} s^{-1}. The LogN-LogS relation of these sources can be calculated from the number of detected sources and the area surveyed for each flux. In the soft band, we obtained the LogN-LogS relation a little different from the past results by the Einstein and the ROSAT Galactic plane surveys, which is reasonably considered from the difference of the area surveyed. In the hard band, the LogN-LogS relation of the faint Galactic sources was derived for the first time in this survey, which is shown in figure 2. It is significantly flatter than a power-law with an index of -1, expected for the two-dimensional source distribution. Thus, it implies that the spatial distribution of the X-ray sources have a one-dimensional structure associated with the Galactic arm and/or the LogN-LogS relation reflect the luminosity function rather than the spatial distribution (Sugizaki 1999).

Finally, we analyzed a small scale spatial fluctuation of the unresolved emission in the 2–10 keV band, which is almost transparent in the Galactic ISM and consists of the GRXE and the cosmic X-ray background (CXB). We fit the model of the uniform surface brightness to raw data after masking the resolved sources and subtracting the large scale intensity variation. The fit could not be accepted. We carefully estimated contributions of various unmodelized effects, which are residuals of the large-scale intensity variation, difference of the effective exposure time, contamination of the extended PSF, stray lights from the bright sources outside of the FOV, and uncertainty of the response function. As the result, we confirmed that a significant residual still remains. We evaluated the fluctuation of the CXB expected from the LogN-LogS relation of the extragalactic sources (Ueda et al. 1999), and found that it can explain the observed residual fluctuation (Sugizaki 1999). Therefore, a fluctuation responsible for the GRXE is not necessarily required. It strictly constrain the unresolved faint sources as the origin of the GRXE. We construct a model of the source distribution on the 4-kpc arm of the Galaxy to explain the GRXE and derived a required condition: their averaged luminosity should be smaller than 1.6×10^{31} ergs s^{-1}and their number density is 0.7×10^{-3} pc^{-3} with a 90% confidence limit (Sugizaki 1999). That condition is illustrated in the figure 2.

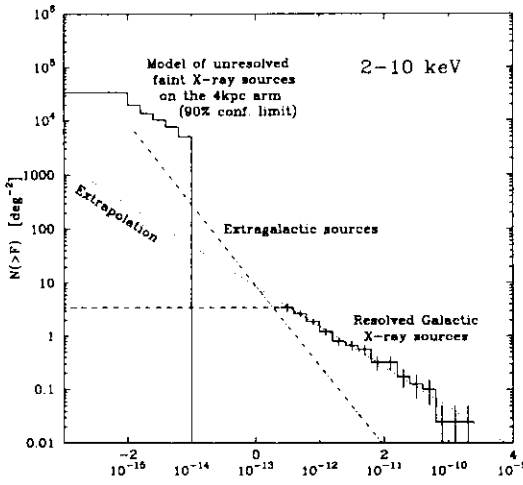

FIGURE 2. The LogN-LogS relation of the Galactic X-ray sources resolved by the ASCA survey in the 2–10 keV band and the allowed model for the unresolved faint sources within the 90% confidence limit from the fluctuation analysis. The LogN-LogS relation of the extragalactic sources observed through the Galactic absorption is shown together, which is estimated form the results of the ASCA LSS (Ueda et al. 1999).

3. DISCUSSION — ORIGIN OF THE RIDGE X-RAY EMISSION

From a similarity of the spectrum with the GRXE, young supernova remnant (SNR), cataclysmic variables (CVs) and massive stars are considered as the candidates. We can estimate the population of the young SNRs from the birth-rate and the evolution of the supernova in the Galaxy. The number of SNRs with a temperature above $\sim 10^8$ K is at most $\sim 10^2$ (Koyama et al. 1986), which cannot explain the spatial uniformity of the GRXE. A population of CVs was estimated only in the nearby solar systems (Patterson 1985), which is $\sim 10^{-6}$ [pc^{-3}], then much smaller by three order of magnitude than that required for the 100% GRXE. We cannot reject a hypothesis that the CVs' density inner the 4 kpc arm is larger than that in the nearby solar systems, however it seems very difficult from the stellar evolution in the Galaxy. Also, recent ASCA observations suggest that some massive stars have a hot plasma with a temperature of $\sim 10^8$ K (Matsuzaki 1999). If all massive stars in the Galaxy have such a hot plasma, the number of sources to explain the full GRXE is satisfied. However, a ratio of those massive stars is very short. Therefore, the hypothesis of diffuse hot plasma as the origin of the GRXE is more plausible even if it has a large problem; how such a hot plasma is produced and confined on the Galactic plane. Magnetic fields and low-energy cosmic rays, whose comprehensive properties in the Galaxy have not been acknowledged, might play important rolls (Kaneda et al. 1997; Varinia & Marshall 1998).

REFERENCES

Kaneda, K., et al. ApJ, 491, 638-652, (1997)
Koyama, K., Ikeuchi, S., & Tomisaka,K. PASJ, 38, 503 (1986)
Matsuzaki, K. Ph.D Thesis Univ. of Tokyo (1999)
Patterson, J. & Raymond, J. C. ApJ, 292, 535-549 (1985)
Sugizaki, M. Ph.D Thesis Univ. of Tokyo (1999)
Ueda, Y., et al. ApJ, 518, 656 (1999)
Warwick, R. S. et al. Nature, 317, 218-221 (1985)

X-RAY EVIDENCE OF AN AGN IN M82

H. Matsumoto [1], T.G. Tsuru [2]

1)CSR/MIT, 77 Massachusetts Avenue, Cambridge, MA 02139-4307, USA
2)Department of Physics, Kyoto University, Kyoto 606-8502, Japan

ABSTRACT

M82, which is the most famous starburst galaxy shows hard X-ray emission. The origin of the hard component, however, has been unclear. Therefore, we conducted a monitoring observation of M82 with ASCA in 1996. A significant time variability of the hard component was found between 3×10^{40} erg/s and 1×10^{41} erg/s on various time scales from 10ks to a month. This strongly suggests that a low-luminosity AGN (LLAGN) exists in M82. A broad iron line emission was found, which is similar to other LLAGNs.

KEYWORDS: galaxies:active — galaxies:starburst — galaxies:individual (M82)

1. INTRODUCTION

Since M82 is thought to be an archetypical starburst galaxy, many X-ray observations of M82 have been made. The first observation of M82 with ASCA was conducted in 1993. Tsuru et al. (1997) analyzed the ASCA spectrum, and found that it consists of three components: soft, medium, and hard. Since the soft and medium components show emission lines from various elements and their X-ray images are extended compared with the ASCA point spread function (PSF), their origin can be thought to be the galactic wind driven by stellar winds from massive stars and supernovae.

The ASCA spectrum of the hard component can be well-described by either a power-law model (the photon index is $\Gamma \sim 1.7$) or a thermal plasma model (the temperature is $kT \sim 14$ keV). Tsuru et al. (1997) compared the ASCA flux in the 2 – 10 keV band with those of Ginga (Tsuru 1992) and EXOSAT (Schaaf et al. 1989), and found a time variability. Furthermore, the spatial extent of the hard component is consistent with the ASCA PSF. These may suggest that the origin of the hard component is a low-luminosity AGN (LLAGN) of M82. However, since Ginga and EXOSAT are non-imaging detectors, possible contamination from other hard sources is not excluded. Furthermore, the Ginga spectrum can be fitted with a thermal model, but cannot be fitted with a power-law model (Tsuru 1992), which is different from the typical X-ray spectra of AGNs. The same conclusion was suggested by Cappi et al. (1999) using the BeppoSAX data. Thus, the origin of the hard component is still debatable.

The first key to revealing the origin of the hard component is to clarify whether or not it shows a time variability. The second key is to detect the iron K-line emission and to determine its central energy. The central energy of the line can be direct evidence. For these purposes, we made a monitoring observation (9 times) of M82 with ASCA in 1996. For more details about the observation and our results, please read Matsumoto and Tsuru (1999) and Ptak and Griffiths (1999).

2. LIGHT CURVE

First, we studied the light curve of each observation. We found that the data on April 24, 1996, shows short-term variability only in the hard-energy band, which is shown in figure 1. The time scale is about 10^4 s. We found no short-term variability in the other observations.

Next, we compared the average counting rate of each observation, which is shown in figure 2. We can see that only the light curves in the high-energy band show time variability.

These light curves strongly suggest that only the hard component of M82 has time variability.

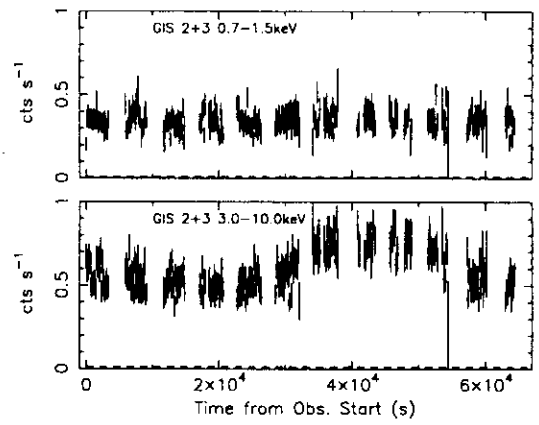

FIGURE 1. Light curves of the GIS2+3 during the observation on April 24, 1996. The background levels are indicated by the dashed lines.

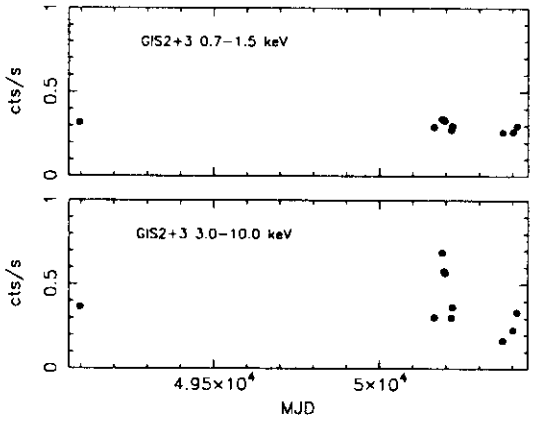

FIGURE 2. Average counting rates of the GIS 2+3.

3. SPECTRAL ANALYSIS

Then we fitted the ASCA spectrum of each observation with the three-temperature thermal plasma model proposed by Tsuru et al. (1997). For the soft and medium components, we fixed their spectral shapes to the best-fit results of Tsuru et al. (1997). Therefore, only their normalizations are free parameters. For the hard component, the free parameters are its absorption column density, temperature, metal-

licity, and normalization. This three-temperature model can fit the spectra of all observations quite well. The X-ray luminosity of each component in the 0.5 – 10 keV band is shown in figure 3. It is clear that only the hard component shows time variability. The temperature of the hard component also changed. However, we found no correlations between the temperature and luminosity of the hard component.

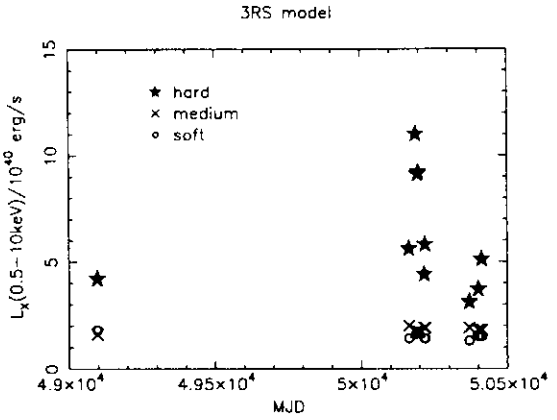

FIGURE 3. Time variability of each component in the three-temperature model. The stars, crosses, and circles show the hard, medium, and soft components, respectively.

We subtracted the spectrum of the lowest state (Apr. 15, 1996) from that of the highest state (Oct. 14, 1996), which is shown in figure 4. This spectrum can be fitted by the heavily absorbed ($N_{\rm H} \sim 10^{21}{\rm cm}^{-2}$) thermal plasma model. This strong absorption suggests that the variable source is embedded in the center of M82.

Finally, we examined the iron line feature. Because the statistics of each observation were rather limited, we combined the spectra of all observations above the 4 keV band. The spectrum can be fitted by the thermal bremsstrahlung continuum plus a Gaussian line model, which is shown in figure 5. The significance of the detection of the Gaussian line is larger than 99%. The center energy, sigma, and equivalent width of the line are 6.56 ± 0.14 keV, 0.30 ± 0.18 keV, and 121 ± 60 eV, respectively (errors are at 90% confidence level). The broad iron line feature is similar to other LLAGNs such as M81 (Ishisaki et al. 1996).

4. CONCLUSION

We found that the hard component of M82 shows time variability between 3×10^{40} erg/s and 1×10^{41} erg/s at various time scales from 10 ks to one month. The variable source shows a heavily absorbed feature with a column density of 10^{21} cm^{-2}, which means the variable source is embedded in the center of M82. Furthermore, the X-ray images of the hard component are consistent with a point source. All these suggest that there is an LLAGN in M82. We also found a broad iron K line, which

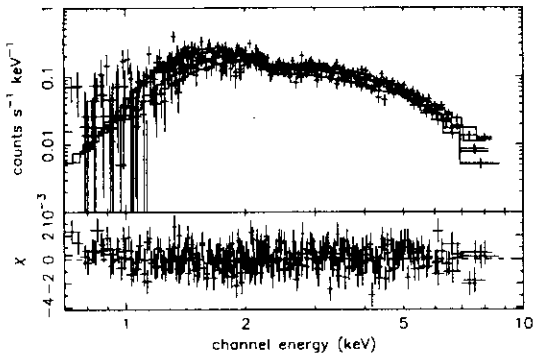

FIGURE 4. Residual SIS and GIS spectra obtained by subtracting the lowest state (Apr. 15, 1996) from the highest state (Oct. 14, 1996). The lines show the best-fit heavily absorbed thermal plasma model.

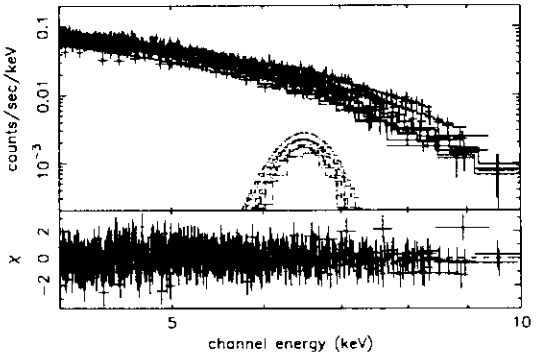

FIGURE 5.
Composite SIS and GIS spectra above the 4keV band. The lines show the best-fitting thermal bremsstrahlung plus Gaussian line model.

is similar to other LLAGNs. Assuming that the origin of the hard component is the LLAGN and the X-rays are mainly emitted from a region as large as 6 times its Schwarzschild radius, the mass of the central object is estimated to be less than $2\times10^8 M_\odot$. This first firm evidence of a LLAGN in M82 suggests a link between starbursts and AGN.

ACKNOWLEDGEMENTS

We thank the ASCA team members for their support. We are also grateful to Miss Deborah Gage for careful review of the manuscript. HM is supported by the JSPS Postdoctoral Fellowships for Research Abroad.

REFERENCES

Cappi, M. et al. 1998, A&A, in print
Ishisaki, Y. et al. 1996, PASJ, 48, 237, 1996
Matsumoto, H., Tsuru, T. G. 1999, PASJ, 51, 321
Ptak, A., Griffiths R. 1999, ApJ, 517, L85
Schaaf, R., Pietsch, W., Biermann, P. L., Kronberg, P. P., Schmutzler, T. 1989, ApJ, 336, 722
Tsuru, T. G. 1992, PhD Thesis, The University of Tokyo
Tsuru, T. G., Awaki, H., Koyama, K., Ptak, A. 1997, PASJ, 49, 619

VARIABILITY OF AN IRON LINE PROFILE AND A POWER-LAW CONTINUUM

K. Misaki[1], H. Kunieda[1], Y. Terashima[2]

1) Department of Physics, Nagoya University, Furo-cho, Chikusa, Nagoya 464-8602, Japan (e-mail address : misaki@u.phys.nagoya-u.ac.jp)
2) Laboratory for High Energy Astrophysics, NASA Goddard Space Flight Center, Code 662, Greenbelt, MD20771, USA

ABSTRACT The iron lines from Seyfert 1 galaxies exhibit broad red-wings in general, which are attributed to the relativistic accretion disk close to the black hole. The line profile provides us with the information of the geometry of the accretion disk and the central source. We examine a time behavior of the iron line in accordance with a spectral variability of the power-law continuum from bright Seyfert galaxy Mrk 841 observed with *ASCA*. The emission mechanism and the structure around a black hole are discussed to accommodate both the spectral change of the continuum and the line profile change.

KEYWORDS: galaxies: individual(Mrk 841); galaxies: Seyfert; X-rays: galaxies

1. INTRODUCTION

ASCA observations of Seyfert 1 galaxies have revealed the iron Kα fluorecsent line being extremely broad and skewed to the low energy end (e.g. Tanaka et al. 1995; Nandra et al. 1997). Those feature can be explained with the combined effect of the relativistic Doppler-shift and the gravitational redshift in the deep gravitational potential due to the central massive black holes (Fabian et al. 1989). No plausible alternative explanation has been found for the line shape (Fabian et al. 1995). Broad and asymmetric line profile is strong evidence for the presence of a massive black hole and gives us the information of the vicinity of the black hole. On the X-ray continuum, the general tendency has been known that Seyferts show the softer spectrum when they are brighter. However, it remains unclear whether the change of the spectral index of the X-ray continuum is the intrinsic change or due to the additional components such as Compton reflection, soft excess, warm absorber.

We report here spectral changes of the luminous Seyfert galaxy Mrk 841 found in two *ASCA* observations, mainly on the change of the iron line profiles. We consider possible scenarios to explain the observed spectral variability. Mrk 841 has shown a violent spectral variability in the previous X-ray observations (George et al. 1993; Nandra et al. 1995). It is one of the best targets to investigate the nature of the X-ray emission and its variability.

the continuum flux is almost same level, doesn't show a drastic change between two observations. The change of the disk can not explain the present phenomena, then the next approach is the change of illumination to the disk. If the illuminating source is assumed to be a point source on axis of the disk, the flux distribution is simply given: $F_X(r) = hL_X/4\pi(r^2+h^2)^{3/2}$ where r is the radius and h is the height of an illuminating source from the disk. When h is negligibly small comparing to r, $F_X(r) \propto r^{-3}$. On the other hand, if the height is much larger than r, $F_X(r) \propto h^{-2}$, then a value of q becomes 0. Therefore, the observed change of the line profile can be explained by the increase of the height of the continuum source. The idea with the change of the source height can be related to the change of the spectral slope in the following scenario. When the soft photon field is strong, the high energy electrons can be frequently scattered by the dense soft photon flux close to the accretion disk. Thus, steeper continuum and broad red-wing would be observed, as is seen in 1993. On the contrary, when the soft photon flux decreases, high energy electrons diverse in larger volume and may have taller distribution above the disk. At the same time, electrons may keep its energy because of much less energy loss by the inverse Compton scattering. Then harder (flatter) X-rays emerge. A similar spectral evolution scenario is suggested from the correlation between the X-ray slope and the strength of Compton reflection (Zdziarski 1998).

Another possibility is a multiple hot spots model, which are not on axis but distributed on the disk. The distribution change of variable hot spots can be inferred from the profile change. For example, many flares happening at outer radii will create a line profile dominated by a narrow component. Iwasawa et al. (1999) suggested this scenario from the variation of the broad iron line profile of MCG $-6-30-15$. In the model of multiple hot spots on the accretion disk, what mechanism causes the spectral slope change? It is not clear that those spots at inner radii emit softer X-rays and vise versa.

ACKNOWLEDGEMENTS

The authors are grateful to all the *ASCA* team members. K. M. and Y. T. thank Japan Society for the Promotion of Science for support. I express special thanks to Dr. K. Iwasawa. He always encourages me and gives us many useful suggestions.

REFERENCES

Fabian, A.C., Rees, M.J., Stella, L., & White, N.E. 1989, MNRAS, 238, 729

Fabian, A.C., et al. 1995, MNRAS, 277, L11

George, I.M., et al. 1993, MNRAS, 260, 111

Iwasawa, K., Fabian, A.C., Young, A.J., Inoue, H., & Matsumoto, C. 1999, astro-ph/9904078

Nandra, K., et al. 1995, MNRAS, 273, 85

Nandra, K., George, I.M., Mushotzky, R.F., Turner, T.J., & Yaqoob, T. 1997, ApJ, 477, 602

Tanaka, Y., et al. 1995, Nature, 375, 659

Zdziarski, A.A. 1999, MNRAS, 303, L11

A NEW EVENT ANALYSIS METHOD FOR THE X-RAY PHOTON COUNT CCD

T.G. Tsuru [1], H. Awaki [1], K. Koyama [1], K. Hamaguchi [1], H. Murakami [1], M. Nishiuchi [1], M. Sakano [1], H .Tsunemi [2]

1) Cosmic Ray Group, Dept. of Physics, Kyoto Univ. Kitashirakawa-Oiwake-Cho, Sakyo, Kyoto, 606-8502, Japan
2) Dept. of Earth and Space Science, Osaka Univ. Machikaneyama-cho, Toyonaka, Osaka, 560-0043, Japan

ABSTRACT We report here a new event analysis method "two-dimensional Gaussian function fitting" for the X-ray photon count CCD camera. A grade method employed in the ASCA satellite is widely used in the event analysis which excluded the extended event as non X-ray event. Our new method can save extended X-ray events without degradation of the energy resolution and without decrease of the background rejection efficiency. It increases the detection efficiency of X-ray photons by 7.5% at 7 keV and 25% at 12.5 keV, respectively. We will employ this method in the X-ray CCD camera onboard ASTRO-E to be launched in February, 2000.

KEYWORDS: Instrumentation: detectors; Methods: data analysis; Techniques: image processing; Techniques: spectroscopic

1. INTRODUCTION

The solid-state imaging spectrometer (SIS hereafter), on-board the ASCA satellite launched in 1993, was the first X-ray photon count CCD camera in space (Tanaka et al. 1994; Burke et al. 1991). Following ASCA, there are three X-ray astronomical satellites in new generation launched around 2000, Chandra, XMM and ASTRO-E, all of which employ X-ray photon count CCD cameras as their standard detector. These X-ray CCDs have thicker depletion layers (50 μm – 300 μm) than that of SIS (35 μm), allowing us to improve the detection efficiency at high energy X-ray. An X-ray photon absorbed shallow inside the CCD produces a small event size (single pixel event and two pixel split event) while that absorbed deep inside the CCD produces an extended charge cloud in the CCD (multi pixels event) as demonstrated in Figure 1. So far, the ASCA grade method is widely used in the data analysis (Gendreau 1995) in which we regard an event extending over 2×2 pixels as non X-ray. It is useful to apply the data for the CCD with relatively thinner depletion layer. However, the CCD with thicker depletion layer will produce X-ray events which are improper to be analyzed by the grade method. Therefore, we developed a new event analysis method "two-dimensional Gaussian function fitting" to handle

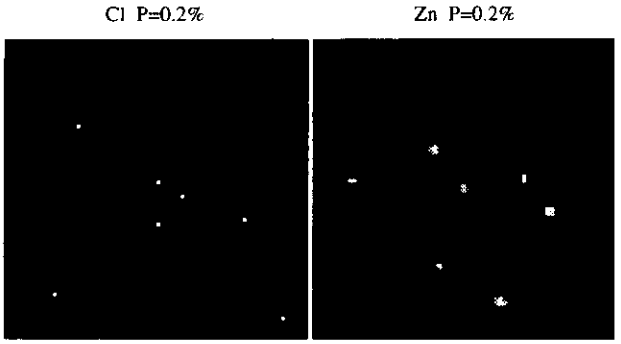

FIGURE 1. The left and right panels show raw frame data of XIS for the chlorine-K line (2.62 keV and 2.82 keV) and the zinc-K line (8.63 keV and 9.57 keV), respectively. Only single pixel events are seen in the figure for the chlorine-K line, while there are some extended events over 2 × 2 pixels for the zinc-K line.

the extended X-ray event properly. This paper describes the introduction and results of this method which will be employed for the X-ray Imaging Spectrometer (XIS hereafter) onboard ASTRO-E (Hayashida et al. 1998; Nishiuchi et al. 1998).

2. THE TWO-DIMENSIONAL GAUSSIAN FUNCTION FITTING METHOD

The new method "two-dimensional Gaussian fitting" is the one in which the 5 × 5 pixel data centered on each event are fitted with a two-dimensional Gaussian function. In this fitting, the center position, normalization and width of the Gaussian function are left as free parameters. The Gaussian function is assumed to be axial symmetric, resulting that the widths in the X- and Y-direction are identical to each other. The pulse height of the event is calculated by integrating the best fit model Gaussian function over the region of 5 × 5 pixels.

2.1. Pulse Height vs. Event Width

The left panel of Figure 2 shows the best fit 1σ width of the Gaussian function (W) as a function of the pulse height (PH) for each illuminated fluorescent X-ray (PH-W diagram hereafter). The distribution for each incident X-ray energy breaks largely at the width of 0.4 pixel (9.6μm).

In the region below the width of 0.4 pixel, the pulse heights of X-ray events are distributed sharply and independent from the width in the horizontal direction, which suggests that the pulse heights of such events are represented well by the fitting method. Figure 2 shows that the relative number of events with large widths for the chlorine-K line is smallest when compared with the other X-ray energies. Since the X-ray energy of the chlorine-K line (2.62 and 2.82 keV) is just above the silicone edge of 1.846 keV, its attenuation length in the CCD is smallest among those of the X-ray energies we illuminated. Therefore, this result suggest that the event with large width is produced by X-ray event absorbed deep inside the CCD.

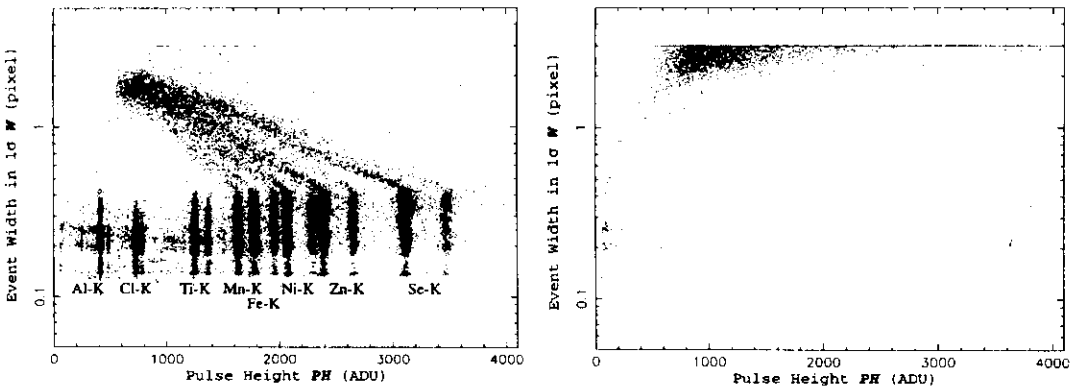

FIGURE 2. The correlation between the event pulse height and the width of the best-fit Gaussian function when illuminated various X-ray energies (left) and ^{60}Co as a non X-ray background simulator (right). The event pulse height is obtained by integrating the best-fit model function over 5×5 pixels.

In the region above the width of 0.4 pixel, the pulse height of an X-ray event becomes smaller as the width increases. Expanding the integration region of the Gaussian function from 5×5 pixels to 11×11 pixels changes this diagram little. Thus, such an largely extended event is thought to be produced by an X-ray absorbed in the field free region and loses some of its electron-hole pairs by recombination (Hopkinson 1983; Hopkinson 1987). The event with the width of 0.4 pixel is produced just at the boundary between the depletion layer and the field free region of the CCD. The properties of these X-ray events will be described in the next paper (Murakami et al. 1999).

The right panel of Figure 2 shows the diagram obtained by illumination of ~ 1 MeV γ-rays from ^{60}Co, which is often used for non X-ray background simulation. The correlation for the γ-rays is very different from that for X-rays. Thus, the PH-W diagram is also useful for non X-ray background rejection.

2.2. Improvement of Quantum Efficiency

We obtained the X-ray energy resolution and quantum efficiency for each X-ray energy from the events with the width smaller than 0.4 pixel. We found that the quantum efficiency increases by 9% at 13 keV without any degradation of energy resolution compared with the ASCA grade method.

Many events are still left unused in the region above the width of 0.4 pixel. We then try to utilize somehow extended events in the region between widths of 0.4 and 0.6 pixel for the improvement of the quantum efficiency. By fitting analytic function to the relationship of PH-W for each incident X-ray energy in this region, we obtained the fraction $f(W, PH)$ of remaining charge after the recombination in the field free region to the initial amount of charge. We next estimated the initial among of charge for each event by dividing PH by $f(W, PH)$. Plotting the

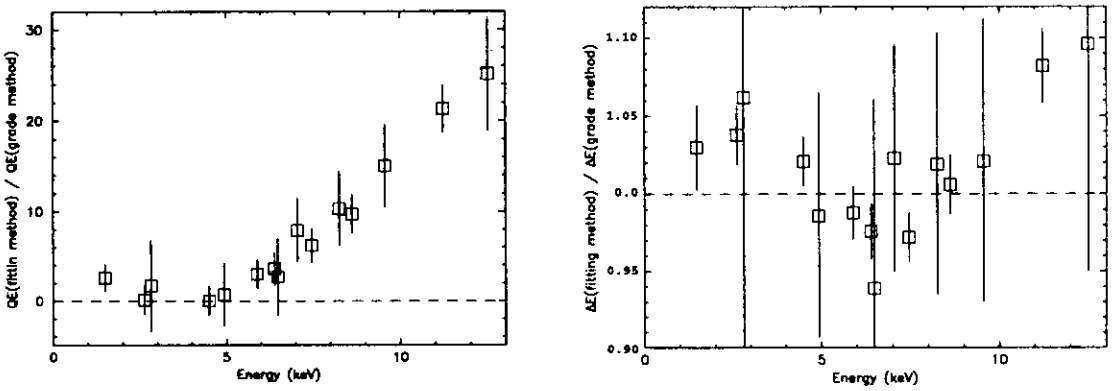

FIGURE 3. The results obtained from events with the width less than 0.6 pixel are displayed. Left: The ratio of the quantum efficiency of the two-dimensional Gaussian fitting method to that of the grade method. Right: The ratio of the energy resolution of the two-dimensional Gaussian fitting method to that of the grade method.

estimated initial amount of charge in the diagram again through this method, we finally obtained X-ray spectra from this "recovered" *PH-W* diagram.

The ratio of the quantum efficiency obtained with this method to that with the ASCA grade method in the left panel of Figure 3, where the quantum efficiency increases by 7.5% at 7 keV and 25% at 12.5 keV, respectively. On the other hand, there is little degradation of energy resolution (the right panel of Figure 3). Thus, it is concluded that the two-dimensional Gaussian fitting method is useful for the increase of the quantum efficiency of an X-ray CCD camera without degrading its energy resolution.

3. CONCLUSION

The two-dimensional Gaussian fitting method newly introduced in this paper gives us higher quantum efficiency by 7.5% at 7 keV and 25% at 12.5 keV without the degradation of the energy resolution compared with the grade method.

REFERENCES

Burke, B.E., Mountain, R.W., Harrison,D.C., et al. 1991, IEEE Trans. ED-38, 1069

Gendreau, K.C. 1995, Ph D. Theses, MIT

Hayashida, K., Kitamoto, S., Miyata, E., et al. 1998, Proc. SPIE, 3445, 278.

Hopkinson, G.R. 1983, NIM, 216, 423.

Hopkinson, G.R. 1987, Optical Engineering, 26, No.8

Nishiuchi, M., Koyama, K., Tsuru, T. et al. 1998, Proc. SPIE, 3445, 268.

Murakami, H. et al. 1999, in preparetion.

Tanaka, T., Inoue, H., Holt, S.S., 1994, PASJ 46, L37